Wang *et al.*
Cell Communication and Signaling (2024) 22:539
https://doi.org/10.1186/s12964-024-01923-0

Cell Communication and Signaling

RESEARCH

Open Access

Novel Ser74 of NF-κB/IκBα phosphorylated by MAPK/ERK regulates temperature adaptation in oysters

Chaogang Wang[1,3,5†], Zhuxiang Jiang[3,5,6†], Mingyang Du[3,5,6], Rihao Cong[2,3,5,8], Wei Wang[3,4,5], Taiping Zhang[3,5,6], Jincheng Chen[3,5,6], Guofan Zhang[1,2,3,5,7,8] and Li Li[1,3,4,5,6,7*]

Abstract

Phosphorylation of Ser32 and Ser36 controls the degradation of IκBα is the conserved cascade mechanisms of immune core signaling pathway, NF-κB pathway in metazoans, but it's response to abiotic stress and the presence of novel phosphorylation mechanisms in other species remain unclear. Herein, we reported a novel heat-induced phosphorylation site (Ser74) at oysters' major IκBα, which independently regulated ubiquitination-proteasome degradation without the requirement of phosphorylation at S32 and S36. And this site was phosphorylated by ERK/MAPK pathway, which then promoted REL nuclear translocation to activate cell survival related genes to defend heat-stress. The MAPK-NF-κB cascade exhibited divergent thermal responses and adaptation patterns between two congeneric oyster species with differential habitat temperatures, indicating its involvement in shaping temperature adaptation. This study demonstrated that the existence of complex and unique phosphorylation-mediated signaling transduction mechanism in marine invertebrates, and expanded our understanding of the evolution and function of established classical pathway crosstalk mechanisms.

Keywords NF-κB pathway, MAPK pathway, IκBα, ERK, Temperature Adaptation, Oysters

Background

Studying the regulatory mechanism underlying temperature adaptation is crucial to understanding the impact and adaptive potential of the organism in response to climate change. Protein phosphorylation is a widely studied post-translational modification that regulates protein localization, influences protein–protein interactions, and participates in protein degradation, making it crucial in mediating stress signal transduction under temperature stress across multiple taxonomic groups [1–4]. Temperature is a fundamental abiotic stress factor, which can directly influence metabolic rates, enzyme activity, membrane fluidity, and cellular functions, which activates numerous conserved signaling pathways by mobilizing corresponding kinases and triggering signal cascades through phosphorylation, including AMPK-mTOR [5, 6], PI3K-AKT [7], NF-κB [8, 9], and MAPK [10], etc.

†Chaogang Wang and Zhuxiang Jiang contributed equally to this work.

*Correspondence:
Li Li
lili@qdio.ac.cn
[1] Key Laboratory of Breeding Biotechnology and Sustainable Aquaculture(CAS), Institute of Oceanology, Chinese Academy of Sciences, Qingdao, China
[2] Laboratory for Marine Biology and Biotechnology, Qingdao Marine Science and Technology Center, Qingdao, China
[3] Shandong Province Key Laboratory of Experimental Marine Biology, Institute of Oceanology, Chinese Academy of Sciences, Qingdao, China
[4] Laboratory for Marine Fisheries Science and Food Production Processes, Qingdao Marine Science and Technology Center, Qingdao, China
[5] National and Local Joint Engineering Laboratory of Ecological Mariculture, Qingdao, China
[6] University of Chinese Academy of Sciences, Beijing, China
[7] Shandong Technology Innovation Center of Oyster Seed Industry, Qingdao, China
[8] Southern Marine Science and Engineering Guangdong Laboratory (Zhanjiang), Zhanjiang, China

Studies on phosphorylation in response to temperature stress in mollusks are lacking, as they are currently limited to the measurement of phosphorylation levels of specific proteins within specific pathways, such as SAPK/JNK [11] or p38 MAPK [12] in MAPK pathway, p53 and p21 [13]. To our knowledge, only our previous study has investigated the global phosphoproteomic response to high-temperature stress in mollusks (oysters), revealing a significant upregulation of phosphorylation level at the Ser74 site of an NF-κB/IκB protein under high-temperature stress, which exhibited divergent phosphorylation patterns between two differentially heat-adaptive species [14], while the conserved Ser32 and Ser36 sites showed no phosphorylation modification, suggesting a potential novel temperature-induced phosphorylation regulatory mechanisms in the NF-κB pathway for oysters.

The NF-κB signaling pathway is essential in organisms and crucial in regulating numerous physiological processes, including development, cell apoptosis, and immune response [15–17]. In mammals, the NF-κB/Rel family members can be divided into two subfamilies based on their C-terminal structures: the NF-κB and Rel subfamilies. The Rel subfamily comprises three members: c-Rel, RelA (p65), and RelB, which have their C-terminal domains responsible for transcriptional activation [18–20]. The inhibitors NF-κB (IκB) are considered crucial regulatory factors of the NF-κB signaling pathway [21]. Its core signaling cascade involves the stimulation of IKK complex (comprising IKKβ, IKKα, and NEMO) kinases by pro-inflammatory cytokines, LPS, growth factors, and antigen receptors, phosphorylating IκB (a key regulatory factor in the NF-κB signaling pathway) at the Ser32 and Ser36 sites, which is conserved across various metazoans and can promote its ubiquitination-proteasome degradation [17, 21, 22]. These events cause the nuclear translocation of REL and trigger the activation of downstream gene expression [22, 23]. Over the past decade, the role of NF-κB, which is essential in the antiviral and antibacterial processes for vertebrate and invertebrate cells, has been focused on the study of animal immune defense [16, 17, 21, 24–32]. And current researches has mainly concentrated on its roles in immune diseases [33, 34], inflammation regulation [34], and cancer progression [35] in mammals and arthropods (such as *D. melanogaster*) [15, 31], lacking reports about its response to abiotic stressors, such as temperature. However, several studies have proven that the NF-κB signaling pathway can also be activated by stimuli such as free radicals, reactive oxygen species, and cytokines, which are typical products of temperature stress [36]. Additionally, current studies on phosphorylation-mediated NF-κB regulatory mechanisms in mollusks focus primarily on identifying Rel/NF-κB and IκB homologs and their expression response during biotic stress [25–30, 32, 37]. Therefore, elucidating the function of phosphorylation of novel Ser74 site at IκB, upstream kinase and signaling cascade pathway mediating its phosphorylation, and downstream REL-activated genes during high temperature will bridge the gap of the phosphorylation-mediated signal transduction for the marine invertebrate in response to the stress and will facilitate understanding the importance and complexity of phosphorylation regulation in temperature adaptation.

Oysters, as representative species with early deciphered genomes in mollusks, are distributed worldwide and possess significant economic and ecological values [38, 39]. Furthermore, oysters inhabit the excessively stressful intertidal zone, which has caused the evolution of perfect tolerance to such conditions [40], making them an ideal model organism for revealing the regulatory mechanisms underlying stress adaptation mediated by specific signaling pathways in mollusks. *Crassostrea gigas* (*C. gigas*) and *Crassostrea angulata* (*C. angulata*) are two allopatric congeneric oyster species that adapt to relatively cold and warm habitats (Northern and Southern China coasts), respectively, exhibiting divergent temperature adaptation [41–45]. Previous study has found differential protein phosphorylation patterns in response to high-temperature stress between *C. gigas* and *C. angulata* [14]. Particularly, opposite phosphorylation levels have been observed in IκB (Ser74) suggesting that NF-κB/IκBα phosphorylation may be crucial in shaping divergent temperature adaptation between the oyster species. Therefore, comparative studies between these two species will facilitate revealing the phosphorylation mechanism of the NF-κB/IκB (Ser74) pathway and its cascade network in mollusks and the role of its phosphorylation regulation in shaping divergent temperature adaptation.

In this study, we reported a novel heat-induced phosphorylation site (Ser74) at major *Cg*IκBα of immune core NF-κB pathway, which had a distinct function independent of the Ser32 and Ser36 sites in mediating its ubiquitin–proteasome degradation and thermal stability. Further functional validation experiments confirmed that this site was phosphorylated by MAPK/*Cg*ERK1/2 kinase, and activated cell survival, fatty acid metabolism, protein translation, and antioxidant gene expression by promoting *Cg*REL nuclear translocation, thereby helping organisms withstand heat stress. And this pathway was regulated by the classical MAPK pathway through the phosphorylation. The MAPK-NF-κB cascade exhibited differential temperature responses and adaptation patterns, which suggests their involvement in shaping the divergent temperature adaptation. Our findings reveal the existence of complex and unique phosphorylation-mediated signal transduction mechanisms in marine

invertebrates, such as oysters, and expand the understanding of the evolution and function of the established classical pathways crosstalk in temperature adaptation.

Methods

Animal material

Wild adult oyster of *C. gigas* and *C. angulata* were collected from their natural habitat in Qingdao (35°44′ N) and Xiamen (24°33′ N), respectively, and used as broodstock [45]. The one-generation common garden experiment was conducted to alleviate the environmental effects [46]. Artificial breeding program including broodstock conditioning, fertilization, and larval cultures, all of which were conducted in hatchery with 22–26°C and 31 ± 1 ‰ seawater. Briefly, the eggs of 30 mature females were mixed and divided into 30 beakers for each species, each fertilized with sperm from one of the 30 males, to maximize parental contribution. Juvenile F_1 progeny (8 months old) of each species were separated into two groups: one group was deployed at the northern site (35°44′N, Qingdao, Shandong province, China) and the other group was deployed at the southern site (24°33′N, Xiamen, Fujian Province, China). Three wo months later, 10-month-old oysters were sampled from each site or collected to laboratory for subsequent studies. The sea water at two sites was recorded using HOBO Conductivity U24 Data Loggers with a time interval of 2 h during November 2021-January 2022.

Phylogenetic analysis

Each member of human IκB family was retrieved from the National Center for Biotechnology Information (NCBI) database. Using TBtools Blast with an E-value threshold of 10^{-5}, a BLASTP analysis was performed to identify all possible NF-κB proteins in the oyster and other species' amino acid sequence databases [47]. Then, the selected proteins were subjected to ANK domain identification using SMART (Simple Modular Architecture Research Tool) (http://smart.emblheidelberg.de) software with default parameters. And the non-IκB family proteins were manually removed based on results of domain identification above. The maximum likelihood phylogenetic tree was reconstructed using PhyloSuite 1.2.2 software [48], incorporating the inferred amino acid sequences of all putative NF-κB family genes in invertebrates, as well as the ERK gene in oysters, and representative genes from vertebrates such as humans. Sequences alignments were conducted using PRALINE software (http://www.ibi.vu.nl/programs/pralinewww/) with default parameters, and poorly aligned sequences and gaps were removed using Gblocks 9.1b (http://www.phylogeny.fr/one_task.cgi?task_type=gblocks) with the following parameter settings: minimum number of sequences for a conserved/flank position (33/33 (NF-κB); 11/11 (ERK)), maximum number of contiguous non-conserved positions (8), minimum length of a block (10), allowed gap positions (with half). The optimal models were tested by ModelFinder [49], and the LG + G4 model (NF-κB) and LG + I + G4 model (ERK) were selected for multi-species tree reconstruction. IQ-TREE integrated into PhyloSuite was used for maximum likelihood tree construction with 20000 ultrafast bootstraps [50]. See Table S1 for details.

Oysters IκB gene expression analysis

The raw sequencing data of the transcriptomes of oysters from different tissues, developmental stages, and under different stress conditions were obtained from Short Read Archive (SRA) (http://www.ncbi.nlm.nih.gov/sra) database (SRP014559; SRP019967) using fastq-dump of SRA-toolkit: fastq-dump -v –split-3 –gzip SRP014559/SRP019967 [38, 51]. The data were aligned to the updated genome of *Crassostrea gigas* (GenBank accession no. GCA_011032805.1) [52] and calculated using Salmon software v0.11.2 (https://combine-lab.github.io/salmon/) in quasi-mapping-based alignment mode with default parameters [53]. First, we established an index for the transcriptome sequence file of *Crassostrea gigas*: salmon index -t C.gigas.transcript.fa -i C.gigas.salmon. Then, we aligned the transcriptome raw data to the reference genome to obtain the expression of each gene: salmon quant –gcBias -l A -1 SRP014559/SRP019967_1.fq.gz -2 SRP014559/SRP019967_2.fq.gz -i C.gigas.salmon -g genome.gtf -o SRP014559/SRP019967.salmon.count -p 4. Heatmap was generated using the OmicShare tools (https://www.omicshare.com/tools).

Molecular evolutionary analyses and ancestral reconstruction

The PAML 4.10.6 software package [54] and its user interface PAMLX [55] were used to analyze the levels of selective pressure acting upon the Mollusca IκBα proteins. Firstly, the PAML branch model was employed to investigate whether the specific branch containing the IκBα proteins with the conserved S74 site in oyster is under selection in mollusks. The one-ratio model assumes a common dN/dS ratio for all branches, while the two-ratio model assumes that the branch of interest has a different ratio of nonsynonymous to synonymous substitutions (dN/dS; ω1) compared to the background ratio (dN/dS; ω0). Then, the random sites models (M1a, M2a, M3, M7, M8, M8a) implemented in the CODEML program were used to estimate the evolutionary rates (dN/dS) at site 179 (*C. gigas* IκBα like4 S74) within mollusk IκBα proteins. Significant differences in model fits were determined by likelihood ratio tests.

Oysters immunohistochemistry

Rabbit polyclonal antibodies against *Cg*REL1 and *Cg*REL2 were generated by Wuhan Bqbio Biological Technology, China. Immunohistochemical staining was performed according to following protocol. The gill tissues of *C. gigas* and *C. angulata* under control and heat stress treatments were fixed and embedded by paraffin (Servicebio, China). Then, the sections were de-waxed and rehydrated. Antigen was retrieved using Tris–EDTA antigen retrieval solution (PH9.0) at 37°C for 15 min (Servicebio, China). The solution of 3% H_2O_2 was used to block the activity of endogenous peroxidase. Antibodies to *Cg*REL1 and *Cg*REL2 were added and incubated overnight at 4°C. HRP-conjugated goat anti-rabbit secondary antibody was then added and incubated for 50 min at room temperature, following by color development with a DAB Chromogen Kit (Servicebio, China). Nuclei were shown with hematoxylin counterstain (Servicebio, China).

Oysters RNAi experiment

Small interfering RNA (siRNA) was synthesized by GenePharma (Shanghai, China) and used for the RNAi experiment (sequences of the siRNA were shown in Table S2). The RNAi experiment was based on our previous study [45]. Briefly, oysters (*C. gigas*) were cleaned and reared in 500 L tank for one week. Then, individuals were anesthetized (500 g MgCl2 + 5 L seawater + 5 L freshwater) and injected with 100 μl of 10 μg/100 μl siRNA (siRNA group, $n = 15$), 10 μg/100 μl NC strands (NC group, $n = 15$) and 100 μl seawater (water group, $n = 15$). Based on the results of the pilot experiment, we selected the most effective siRNA and interference time. In the formal experiment, gill tissue was sampled from 15 individuals in each group at 24 h post-injection for subsequent RNA extraction and qRT-PCR. Meanwhile, a continuous heat stress experiment was performed at 42°C (sublethal temperature), and the mortality of oysters was recorded hourly. Survival curves were analyzed and plotted based on the Kaplan–Meier method using GraphPad Prism version 8.0.2 for Windows.

RNA-seq after RNAi experiment

RNA extraction from gill tissues of *C. gigas* in RNAi experiment was performed using TRIzol reagent (Tsingke Biotechnology, China). Every five samples were pooled in equal quantities to form a single biological replicate. The NEBNext Ultra™ RNA Library Prep Kit for Illumina (NEB, USA) was used for generating the RNA-Seq library for each sample, which was then subjected to sequencing on the NovaSeq 6000 platform. To ensure the acquisition of high-quality and clean reads, Trimmomatic software (v0.36) [56] was implemented to eliminate adapter sequences, reads containing 10% of unknown nucleotides (N), and reads with more than 50% low-quality bases (Q-value ≤ 20). Subsequently, the clean reads were aligned to the oyster genome (GenBank accession no. GCA_011032805.1) [52] using HISAT2 v2.1.0 [57]. The HTSeq v0.6.0 tool was used to count the reads for each gene in each sample to quantify gene expression [58]. The DESeq2 R package (v1.6.3) [59] was utilized to identify statistically significant changes in gene expression (q-value ≤ 0.05 and |log2(fold change)| ≥ 1). The sequencing data in this study has been deposited into the Sequence Read Archive (SRA) BioProject, under the accession number PRJNA1059049.

DAP-seq

The full-length CDSs of *CgRel1* and *CgRel2* were ligated with pFN19K HaloTag® T7 SP6 Flexi® Vector using ClonExpress II One Step Cloning Kit (Vazyme Biotech, China). Gene Denovo Biotechnology Co. (Guangzhou, China) submitted recombinant vectors for the *in vitro* expression of candidate proteins and conducted DNA affinity purification sequencing (DAP-seq) [60]. The genomic DNA was extracted from the gill tissue of *C. gigas*. The DNA was then sonicated to generate fragments of approximately 200 bp in length, followed by the construction of a DNA library using magnetic bead-based size selection. Recombinant proteins were subsequently immobilized on magnetic beads and mixed with the DNA library. Eluents were then used for PCR amplification and bead purification. The resulting products were sequenced using the Illumina HiSeq™ 4000. Raw reads were processed to obtain clean reads by removing reads containing adapters and low-quality reads, which were then aligned to the oyster genome (GenBank accession no. GCA_011032805.1) [52] using the Bowtie2 software (v2.2.5) [61]. DeepTools (v3.2.0) was employed to determine read counts within the intervals spanning from transcription start sites (TSS) to transcription end sites (TES), as well as the upstream and downstream 2-kb intervals [62]. The DAP-seq data was subsequently analyzed using the MACS2 software (v2.1.2) [63] to identify regions of enriched reads. The dynamic Poisson distribution was used to calculate *p*-value based on the read counts from uniquely mapped reads within specific regions. Regions with a q-value of 0.05 were considered as peaks. The ChIPseeker R package was employed to annotate the peak-related genes [64]. The distribution of peaks across genomic regions, including intergenic, introns, downstream, upstream, and exons was analyzed. The sequencing data in this study has been deposited into the Sequence Read Archive (SRA) BioProject, under the accession number PRJNA1058704.

Differential Scanning Fluorimetry (DSF)

The recombinant purified proteins, His-*Cg*IκBα and His-*Cg*IκBα^{S74A} were utilized for performing Differential Scanning Fluorimetry (DSF) experiment to assess the influence of Ser74 site phosphorylation on protein thermal stability. DSF was performed using 10 μM protein and 10X SYPRO Orange (Invitrogen, USA). The samples were subjected to a heating ramp from 25°C to 95°C at a rate of 1°C/s using the ABI 7500 Fast Real-Time PCR System (Applied Biosystems, USA). Data was analyzed by Protein Thermal Shift Software v1.4 to obtain melting temperature (Tm).

Oyster heat stress raw data reanalysis

The transcriptomic, ATAC-Seq, and protein phosphorylation omics data for *C. gigas* and *C. angulata* under 12 h of heat stress were obtained from our previous study. The ATAC-Seq signals in target region were calculated using DeepTools (v3.2.0) [62] and visualized using the Integrated Genomic Viewer (version 2.16.0) [65]. The heatmap were visualized using using the OmicShare tools (https://www.omicshare.com/tools).

Oysters qRT-PCR experiment

Gill tissues from oyster were collected for total RNA extraction using the TRIzol reagent (Tsingke Biotechnology, China). First-strand cDNA was generated using HiScript III RT SuperMix for qPCR (Vazyme Biotech, China). The primers were designed using Primer 5 software and synthesized by Tsingke Biotechnology (detailed sequences of primers were shown in Table S4). The Ef-1α gene was used as an internal control. The qPCR was conducted using the Taq Pro Universal SYBR qPCR Master Mix (Vazyme Biotech, China) in the ABI 7500 Fast Real-Time PCR System (Applied Biosystems, USA). The $2^{-\triangle\triangle CT}$ method was used to calculate the relative expression [66]. The detailed comparison between the two species has been previously described [45].

Co-IP

Co-IP assays were conducted using the Flag-tag Protein IP Assay Kit with Magnetic Beads (Beyotime Biotechnology, China). Total RNA was extracted from *C. gigas* gill tissues using TRIzol reagent. Then, the first-strand cDNA was synthesized using a HiScript® III 1st Strand cDNA Synthesis Kit (Vazyme Biotech). PCR fragments corresponding to the open reading frames (ORFs) of *CgIκBα*, *CgRel1*, *CgRel2* and *CgErk* were amplified using 2 × Phanta Max Master Mix (Vazyme Biotech) using forward and reverse primers (Table S3), and inserted into pCMV-N-Flag and pCMV-N-Myc plasmids for fusion with the tag. The ligation products were transformed into DH5α competent cells (Tsingke Biotechnology, China) to screen for the presence of recombinants by DNA sequence (Tsingke Biotechnology). Then, the plasmids were purified from DH5α using the SPARKeasy Endofree Midi Plasmid Kit (Shandong Sparkjade Biotechnology, China). HEK293T cells (Procell Life Science & Technology, China) were plated in *10-cm Petri dish* (NEST, China) 1 day before transfection and were cultured under adherent conditions in high-glucose DMEM (Biological Industries, Israel) and 10% fetal bovine serum (Biological Industries, Israel). Cells were transfected with 12.5 μg (per well) plasmid using Lipofectamine 3000 (Invitrogen, USA), and then cultured for 24 h for subsequent Co-IP experiments. The Co-IP reaction was performed according to the manufacturer's instructions. Briefly, the cells lysates were incubated with anti-Flag magnetic beads and Mouse IgG magnetic beads overnight. Following washing step, the reaction products were loaded onto 4 ~ 20% SDS-PAGE gels (GenScript Biotech, China), and then the signals were obtained by western blotting.

Subcellular localization

The full-length CDSs of *CgIκBα*, *CgRel1*, *CgRel2* and *CgErk* were amplified and inserted into pCMV-N-EGFP, pCMV-N-mCherry and pCMV-N-CFP plasmids for fusion with the reporter gene, respectively (Beyotime Biotechnology, China; Table S3). The Lipofectamine 3000 (Invitrogen, USA) was used to transfect these plasmids into HeLa cells (Procell Life Science & Technology, China), which was cultured in RPMI Medium 1640 (Biological Industries, Israel) and 10% fetal bovine serum (Biological Industries, Israel). After 24 h, the HeLa cells were incubation at 42°C for 2 h, the fluorescence was imaged using a confocal microscope LSM710 (Carl Zeiss, Germany).

BiFC assay

The full-length CDSs of *CgIκBα*, *CgRel1*, *CgRel2* and *CgErk* were amplified and inserted into pBiFC-VN173 and pBiFC-VC155 plasmids (MiaoLing Plasmid Platform, China; Table S3). The cell culture, plasmid transfection and imaged for fluorescence as mentioned in the section "Subcellular Localization".

Luciferase reporter assay

The promoter region of *CgRel* downstream genes was amplified and inserted into pGL3-Basic plasmid (MiaoLing Plasmid Platform, China; Table S3). The pRL-TK Renilla luciferase plasmid, pNF-κB-luc (Beyotime Biotechnology, China) or recombinant pGL3 plasmid and different plasmids combinations were transfected into HEK293T cells as above. Luciferase activity was measured using the Dual-Luciferase Reporter Assay System

(Promega, USA) and measured using Varioskan Flash multimode reader (Thermo Fisher Scientific, USA). All experiments were conducted three technical replicates, and the firefly luciferase activity was normalized to the Renilla luciferase activity of each sample.

EMSA

The recombinant plasmids pCMV-N-Myc encoding *CgRel1* and *CgRel2* were transfected into HEK293T cells as above. Cells transfected with pCMV-N-Myc plasmid were utilized as a control, and the cellular nuclear proteins were extracted for the ESMA experiment as mentioned in the section "HEK293T Cells Nuclear and Cytoplasmic Isolation". The biotin-labeled EMSA probe specific to NF-κB and its corresponding unlabeled cold probe were acquired from Beyotime Biotechnology, China. The other DNA probe labeled with 5′ biotin was synthesized by Tsingke Biotechnology, and biotinylated and unlabeled probe sequences were as follows: F, 5′-GGGCAATTAC-3′. For super-shift assay 1ug of anti-Myc antibody (ABclonal, China) was added. Binding reactions, and detection of probe shifts were performed using the LightShift® Chemiluminescent EMSA Kit (Thermo Fisher Scientific, USA) according to the manufacturer's instructions.

Cell apoptosis assay

Cell apoptosis after 2 h of 42°C was analyzed using Annexin V-fluorescein isothiocyanate (FITC) and propidium iodide (PI) apoptosis detection kit (Solarbio, China) according to the manufacturer's instructions. And the apoptotic cells were detected using the FACSAria II flow cytometry (Becton Dickinson, USA). Data was analyzed using FlowJo (version 10.8.1).

Cell Counting Kit-8 (CCK-8) Assay

Cell death after heat stress (42°C, 2 h) was measured using the Enhanced Cell Counting Kit-8 (Beyotime Biotechnology, China) at 36 h after transfection, according to the manufacturer's instructions. The Varioskan Flash multimode reader (Thermo Fisher Scientific, USA) was used to measure the absorbance at 450 nm.

In vivo ubiquitination assay

The *in-vivo* ubiquitination assay was utilized to assess the degree of ubiquitination of the *Cg*IκBα protein at various phosphorylation levels. HEK293T cells were co-transfected with Flag-*CgIκBα* plasmid or its corresponding site-mutated variants, as well as the HA-Ub plasmid (MiaoLing Plasmid Platform, China). Following an 8-h treatment with MG132 (10 μM; MCE, USA), the ubiquitinated IκBα protein was purified using the anti-Flag magnetic beads as mentioned in the section "Co-IP". The purified product was subsequently separated by 4–20% SDS-PAGE and subjected to western blotting.

Yeast two-hybrid assay

The full-length CDSs of *CgIκBα* and *CgErk1/2* were amplified and inserted into pGBK-T7 and pGAD-T7 (MiaoLing Plasmid Platform, China), respectively (Table S3). Pairwise interactions were tested using GAL4 Yeast Two-Hybrid Media Kit (Coolaber, China). Briefly, each vector (bait and prey) was transformed in the Y2HGold yeast strain, and plated first on -Leu -Trp plates to allow selective growth of transformants. After 2–3 days, growth transformants were inoculated into (-Leu, -Trp) medium and allowed to grow overnight at 30°C with continuous shaking at 200 rpm. Subsequently, 10 μl of cell suspension, diluted in ddH_2O to achieve an optical density (OD) of 0.5 and 1.0, was plated on selective plates (-Leu, -Trp), (-Leu, -Trp, -His3) and (-Leu, -Trp, -His3, -Ade2) and incubated for 2–3 days to assess the presence of interactions.

Prediction of kinase

The iGPS1.0 software was utilized for predicting potential kinases targeting the *Cg*IκBα S74 site. This prediction was based on the Short Linear Motif (SLM) theory, which focuses on the surrounding short linear motifs associated with the phosphorylation site (p-site), providing a high degree of specificity [67]. For the analysis, *Homo sapiens* was chosen as the organism, with a threshold set to "medium" and the "interaction" parameter configured as "Exp./String".

In vivo phosphorylation assay

Recombinant Flag-*CgIκBα* plasmid and its site-mutated variants, along with additional upstream plasmids such as Myc-*CgErk1/2* plasmid, were co-transfected into HEK293T cells as above. After 36 h, the cells were lysed using a lysis buffer supplemented with protease and phosphatase inhibitors (Beyotime Biotechnology, China). The IκBα protein was subsequently purified using the anti-Flag magnetic beads as mentioned in the section "Co-IP". The phosphorylation levels of the IκBα protein were then measured using the Phos-tag SDS-PAGE method. Phos-Tag™ was purchased from FUJIFILM Wako Pure Chemical Corporation, Japan and used according to the manufacturer's protocol. Briefly, gels used for Phos-tag SDS-PAGE consisted of a separating gel [8% (w/v) acrylamide, 375 mM Tris–HCl, pH

8.8, 50 μM Phos-tag acrylamide, 100 μM $MnCl_2$, 0.1% SDS solution, 0.1% (v/v) N,N,N′,N′-tetramethylethylenediamine (TEMED), and 0.05% (w/v) ammonium persulfate (APS)], and a stacking gel [4.5% (w/v) acrylamide, 125 mM Tris–HCl, pH 6.8, 0.1% SDS solution, 0.1% (v/v) N,N,N′,N′-tetramethylethylenediamine (TEMED), and 0.05% (w/v) ammonium persulfate (APS)]. Electrophoresis was conducted at a constant current of ≤ 30 mA/gel with the running buffer [25 mM Tris-base, 192 mM glycine, and 0.1% (w/v) SDS]. For western blotting analysis, gel was washed using wash buffer [25 mM Tris, 192 mM glycine, 0.1% (v/v) SDS, 10 mM EDTA] for 10 min three times to remove metal ions, followed by one wash without EDTA for 10 min. Then, the samples were electroblotted to the polyvinylidene difluoride (PVDF) membrane (Millipore, USA) for subsequent western blotting.

In vitro kinase activity assay

The full-length CDSs of *CgIκBα* and *CgErk1/2* and their site-mutated variants, were amplified and inserted into pET-32a plasmid to express the 6 X His-tags at both N- and C-ends (Table S3). The purified proteins were used to test whether recombinant *Cg*ERK1/2 could phosphorylate *Cg*IκBα, as well as to evaluate the influence of phosphorylation at the T187 and Y189 sites of *Cg*ERK12 on its ability to phosphorylate *Cg*IκBα. The wild type and S74A mutant of *Cg*IκBα was used as substrate. The kinase activity assay was performed in 20 μl kinase buffer containing 25 mM Tris–HCl, pH 7.5, 5 mM beta-glycerophosphate, 2 mM dithiothreitol (DTT), 0.1 mM Na_3VO_4, 10 mM $MgCl_2$, 20 mM ATP (CST, USA), 1 μg substrate protein and 1 μg kinase protein for 30 min at 30°C. And the reactions were stopped with SDS loading buffer and electrophoresed on Phos-tag SDS-PAGE as mentioned in the section "*In vivo* Phosphorylation Assay".

Nuclear and cytoplasmic isolation

The HEK293T cells (transfected with Flag-*CgIκBα*, Myc-*CgRel1*, Myc-*CgRel2*, Myc-*CgErk*, and His-*CgMap2k1/2*, and treated with 2 h of 42°C,) and oysters gill tissues (after 12 h of 37°C) were lysed using NE-PER Nuclear and Cytoplasmic Extraction Reagents (Thermo Fisher Scientific, USA) according to manufacturer's instructions. Then, the nuclear and cytoplasmic proteins were loaded onto 4 ~ 20% SDS-PAGE gels and detected using western blotting.

Western blotting

The samples from oysters and cells were extracted using Cell lysis buffer for Western and IP (Beyotime Biotechnology, China) and M-PER™ Mammalian Protein Extraction Reagent containing protease inhibitor (Thermo Fisher Scientific, USA) supplemented with protease and phosphatase inhibitors (Beyotime Biotechnology, China), respectively. The supernatant protein was collected by centrifugation, and then subjected to denaturation at 100°C for 10 min after the addition of 4X protein loading buffer (GenScript Biotech, China). Then, the proteins were transferred onto 0.45 nm pore polyvinylidene fluoride (PVDF) membrane (Millipore, USA) using an eBlot™ L1 wet transfer (GenScript Biotech, China). Membranes were blocked and incubated with primary antibodies and secondary antibodies using eZwest Lite Automated Western Device (GenScript Biotech, China). Membranes were then incubated with Omni-ECL™Femto Light Chemiluminescence Kit (Epizyme, China) and captured using the Molecular Imager® Gel Doc™ XR System (Bio-Rad, USA). The antibodies used were as follows: Flag-tag (ZENBIO, 390002), Myc-tag (ZENBIO, 390003), beta Tubulin (ZENBIO, 200608), Histone H3 (ZENBIO, R24572), beta Actin (ZENBIO, 200068-8F10), HA-tag (ZENBIO, 201113), His-tag (ZENBIO, 230001), ERK1/ERK2 (ABclonal, A16686), Phospho-ERK1-T202/

(See figure on next page.)

Fig. 1 Phylogenetic analysis and sequence alignment of IκB. **A** Phylogenetic tree of IκB genes family from invertebrates and vertebrates. The tree was constructed with the maximum likelihood (ML) method using PhyloSuite. *Cg*REL was chosen for outgroup. Bootstrap support values are indicated by sizes on nodes of phylogenetic tree. The cluster of *Cg*IκB like4 is marked with red dotted lines. Different colors indicate different categories and IκB subfamilies. Purple rectangle represents ANK domain. Hm, *Homo sapiens*; Mm, *Mus musculus*; Dr, *Danio rerio*; Sk, *Saccoglossus kowalevskii*; Sp, *Strongylocentrotus purpuratus*; Dm, *Drosophila melanogaster*; Cg, *Crassostrea gigas*; Ca, *Crassostrea angulata*; Car, *Crassostrea ariakensis*; My, *Mizuhopecten yessoensis*; Bg, *Biomphalaria glabrata*; Hr, *Haliotis rubra*; Ob, *Octopus bimaculoides*; Os, *Octopus sinensis*; Nv, *Nematostella vectensis*; Aq, *Amphimedon queenslandica*. **B** Heatmap of four *C. gigas* IκBα genes' normalized expression (row and column) in different tissues, different developmental stages and under various stress conditions. The relative expression of each gene is indicated by color (from green, low to pink, high). The expression under different stress conditions was all derived from the expression of IκBα in gill tissue. Amu, Adductor; Dgl, Digestive gland; Fgo, Female gonad; Mgo, Male gonad; Gil, Gill; Hem, Hemocyte; Lpa, Labial palp; Man, Mantle; E, egg; TC, Two cells; FC, Four cells; EM, Early morula stage; M, Morula stage; B, Blastula stage; RM, Rotary movement; FS, Free swimming; EG, Early gastrula stage; G, Gastrula stage; T, Trochophore; ED1, Early Dshaped larva; D, Dshaped larva; EU, Early umbo larva; U, Umbo larva; LU, Later umbo larva; P, Competent pediveliger for metamorphosis; S, Spat; J, Juvenile; ppt, Salinity unit (part per thousand); Dy, Drought; Zn, Zinc stress; Cd, Cadmium stress; Zn + Cd, Zinc and Cadmium stress; Cu, Copper stress; Pb, Lead stress; Hg, Mercury stress; Vi, *Vibrio* sp. stress. **C** The sequence alignment of human and oyster IκBα proteins surrounding S74 on *C. gigas* IκBα like4

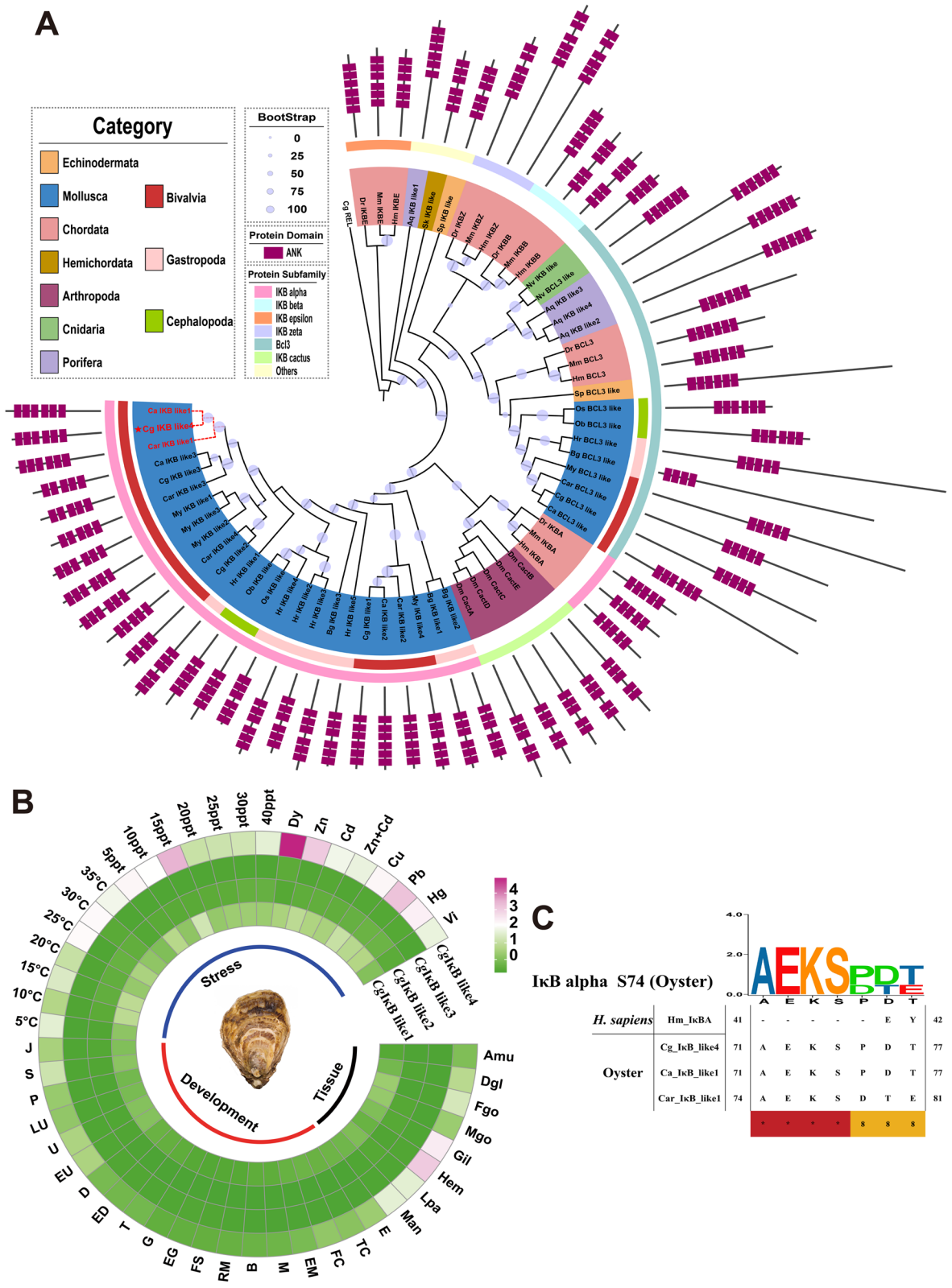

Fig. 1 (See legend on previous page.)

Y204 + ERK2-T185/Y187 (ABclonal, AP0472), MAP2K1/MAP2K2 (ABclonal, A24394), Phospho-MAP2K1-S217/MAP2K2-S221 (ABclonal, AP0209), MAP3K1 (ABclonal, A21490), HRP-labeled Goat Anti-Mouse/Rabbit IgG(H + L) (Epizyme, LF101) and HRP-labeled Goat Anti-Mouse/Rabbit IgG(H + L) (Epizyme, LF102).

Statistical analysis

All statistical analyses were performed using GraphPad Prism version 8.0.2 for Windows. After confirming the normality of the distributions using the Shapiro–Wilk test and homogeneity of variance using Bartlett's test, data were analyzed with the two-tailed unpaired Student's t-test, one-way analysis of variance (ANOVA) and two-way ANOVA followed by Tukey's multiple comparisons test. Data are shown as the means ± SD, and the number of replicates (n) are denoted in the corresponding figure legends. Significant differences between groups were marked with "*" for $P < 0.05$, "**" for $P < 0.01$, "***" for $P < 0.001$ and "****" for $P < 0.001$. The schematic presentation was created using BioRender software (https://biorender.com).

Results

Specific evolution of Ser74 in oyster's major IκBα

The phylogenetic analysis of the IκB protein family across vertebrates and invertebrates revealed that marine mollusks possess only BCL3 and IκBα proteins, accompanied by variations in the number of ANK domains (Table S1, Fig. 1A). Notably, the IκBα protein demonstrated an expansion in copy number in Bivalvia and Gastropoda, such as *C. gigas* had four IκBα proteins. Expression analysis of *C. gigas* demonstrated distinct variations among the four IκBα genes, with *Cg* IκB like4 exhibiting significantly higher expression than the other three IκBα genes. Moreover, the expression of *Cg* IκB like4 displayed tissue specificity, with marked higher expression observed in the gill tissue and hemocyte (Fig. 1B).

Furthermore, *Cg* IκB like4 demonstrated responsiveness to abiotic and biotic stressors, including high temperature and *Vibrio* sp. stress (Fig. 1B). Additionally, the sequence alignment results showed the presence of conserved Ser32 and Ser36 residues in IκBα proteins of marine mollusks (Fig. S1). However, the Ser74 residue is unique to oysters (*Cg* IκBα like4, *Ca* IκBα like1, and *Car* IκBα like1), representing specie-specific site (Fig. 1C). The analysis of selective pressures showed that the significant heterogeneity in the selective constraint levels between the foreground (oyster-specific IκBα proteins) and background (other mollusks IκBα proteins; $P < 0.001$; Table S5) branches based on branch models of PAML. And the oyster-specific IκBα protein ($\omega_1 = 0.00324$) exhibited stronger negative selection than other mollusk IκBα proteins ($\omega_0 = 0.18047$). Further analysis using site models revealed that under the one-ratio model M0, the maximum likelihood estimate for the ω value of the mollusk IκBα genes was calculated as 0.18, indicating that the expansion of IκBα genes in mollusks was subjected to strong purifying selection (Table S6). Moreover, based on the Δ AIC value, M8a emerged as the most suitable site model, suggesting a certain degree of positive selection acting upon the IκBα gene sequences in mollusks; however, no compelling evidence supports the presence of intense positive selection. The ancestral reconstruction analysis revealed that the amino acid variant V179S (*Cg* IκBα like4, Ser74) was introduced at the onset of the oyster branch, signifying it as a site of oyster-specific evolution (Fig. S2). The Bayes empirical Bayes posterior probabilities were calculated as 0.1877, suggesting that this site is not subject to positive selection.

Oyster major IκBα inhibited the nuclear entry of the REL to reduce heat resistance

We conducted inhibitory interaction experiments between *Cg*IκB like4 (subsequently referred to as CgIκBα) and CgREL1/CgREL2 using Co-IP, BiFC,

(See figure on next page.)

Fig. 2 *Cg*IκBα inhibits the nuclear translocation of *Cg*REL and then decreases its heat resistance. **A** Co-immunoprecipitation (co-IP) of *Cg*IκBα with *Cg*REL1/*Cg*REL2. **B** BiFC assay of *Cg*IκBα and *Cg*REL1/*Cg*REL2. Images were acquired with a confocal microscope at the EGFP channel. Bar: 10 μm. **C** Subcellular localization of *Cg*IκBα and *Cg*REL1/*Cg*REL2 in HeLa cells under control and heat stress. Bar: 10 μm. **D** The western blotting of nuclear and cytoplasmic proteins from HEK292T cells transfected with Flag-*CgIκBα* and Myc-*CgRel1*/Myc-*CgRel2* under control and heat treatment. **E** The relative dual-luciferase reporter (DLR) values of HEK293T cells transfected with pNF-κB-Luc, pRL-TK, Myc-*CgRel1*/Myc-*CgRel2* and Flag-*CgIκBα* ($n = 3$). Among these, the transfection amounts of Flag-*CgIκBα* were increased in a gradient manner, with doses of 100 ng, 300 ng, 500 ng, and 700 ng per well of a 24-well plate, respectively. The cell apoptosis rate (**F**; $n = 3$) and the CCK-8 assay for the cell viability (**G**; $n = 5$) of HEK293T cells transfected with Flag-*CgIκBα* and Myc-*CgRel1*/Myc-*CgRel2* under control and heat treatment. The left panel is the cell apoptosis chart in each group, and the right panel is the cell apoptosis rate in each group. **H** The immunohistochemistry of *Cg*REL1 and *Cg*REL2 in gill tissues from *C. gigas* and *C. angulata* under control and heat treatment. **I** The relative expression of oyster *Rel1* and *Rel2* in gill tissues in *Cg*REL RNA interference experiments ($n = 3$). NC, Water, *Rel1*-siRNA and *Rel2*-siRNA in legend represent the oysters were injected with nonsense strands, water, siRNA, respectively. **J** Kaplan–Meier survival curves of oysters in heat-lethal experiments after *Cg*REL RNA interference experiments. Different colors represent oysters injected with nonsense strands, water, siRNA, respectively. The error bars represent the S.D. Significant differences among groups were marked with $^{*}p < 0.05$, $^{**}p < 0.01$, $^{***}p < 0.001$, and $^{****}p < 0.0001$. "ns" indicates non-significant differences

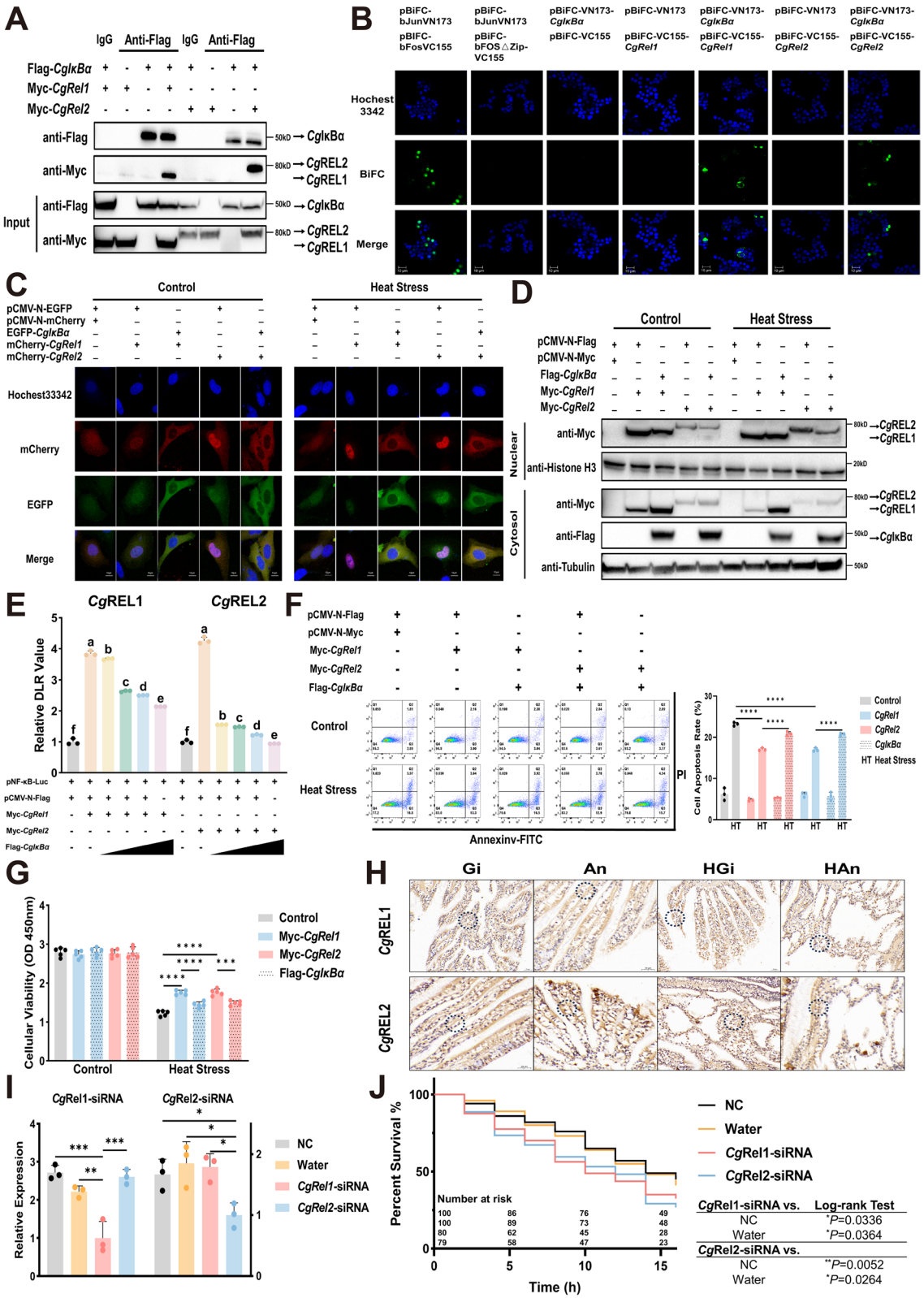

Fig. 2 (See legend on previous page.)

subcellular co-localization, nuclear and cytoplasmic Western blotting, and luciferase reporter experiments based on human cell transfection. The Co-IP result demonstrated the specific interaction between Myc-*Cg*Rel1, Myc-*Cg*Rel2, and Flag-*Cg*IκBα (Fig. 2A). The BiFC result showed the physical interaction between *Cg*REL1, *Cg*REL2, and *Cg*IκBα in the cytoplasm (Fig. 2B). The subcellular localization results demonstrated that, under normal conditions, the *Cg*REL1 and *Cg*REL2 exhibited a diffuse distribution throughout the cytoplasm and nucleus; however, upon co-transfection with *Cg*IκBα, its localization was prominently constrained to the cytoplasm. High-temperature exposure markedly induced a significant increase in the nuclear translocation of the *Cg*REL1 and *Cg*REL2. However, co-transfection with *Cg*IκBα considerably attenuated the nuclear translocation of REL (Fig. 2C). Western blotting revealed a substantial upregulation of *Cg*REL1 and *Cg*REL2 protein levels in the cellular nucleus under thermal stress, whereas co-transfection with *Cg*IκBα caused a notable decrease in REL nuclear translocation (Fig. 2D). The luciferase reporter experiments further supported that *Cg*IκBα can gradiently inhibit the positive transcriptional activity of *Cg*REL1 and *Cg*REL2 on the NF-κB signaling pathway promoter (One-way ANOVA; Fig. 2E). The EMSA experiment demonstrated the binding capability of the *Cg*REL1 and *Cg*REL2 to the NF-κB signaling pathway promoter, and the super shift results (Lanes 4 and 8) provided additional evidence confirming its specific binding (Fig. S3). Subsequently, we conducted cell apoptosis and cell viability experiments based on co-transfection in human cells to investigate the role of *Cg*REL in thermal injury, as well as the inhibitory effect of *Cg*IκBα on it. The cellular heat-induced apoptosis experiments revealed a significant contribution of *Cg*REL1 and *Cg*REL2 in enhancing cellular resistance against high temperature-induced apoptosis ($P < 0.0001$), whereas co-transfection with *Cg*IκBα caused a pronounced REL inhibition, increasing cell apoptosis rate ($P < 0.0001$; Two-way ANOVA; Fig. 2F). The CCK-8 cell viability results corroborated the above findings ($P < 0.001$; Two-way ANOVA; Fig. 2G).

Additionally, we also detected the nuclear translocation of *Cg*REL during oyster heat stress process through immunohistochemistry, and investigated the role of *Cg*REL in oyster heat-induced mortality using RNAi followed by heat stress experiments. Immunohistochemistry further corroborated the heat-induced nuclear translocation of the REL protein in *C. gigas* and *C. angulata* (Fig. 2H). The results of the pilot RNAi experiment indicated that *CgRel1*-1018 (24 h) and *CgRel2*-1813 (24 h) were the most effective siRNA and time for *CgRel1* and *CgRel2*, respectively (Fig. S4). The results of the formal experiment were consistent with those of the pilot experiment, demonstrating that *CgRel1*-1018 and *CgRel2*-1813 specifically knocked down *CgRel1* by 63% and *CgRel2* by 40% compared to NC group, respectively ($P < 0.05$; One-way ANOVA; Fig. 2I). Following the RNAi experiment, we conducted a heat-induced death experiment. The Kaplan–Meier survival analysis demonstrated significantly reduced survival rates in the groups treated with *CgRel1*-1018 (*CgRel1*-siRNA) and *CgRel2*-1813 (*CgRel2*-siRNA groups) compared with the control groups (NC and Water groups; $P < 0.05$; Fig. 2J).

Phosphorylation at Ser74 independently mediated the IκBα degradation

Our previous study found divergent phosphorylation levels at the Ser74 site of the oyster-specific IκBα (*Cg*IκB like4) during heat stress in *C. gigas* and *C. angulata*. *Crassostrea angulata* exhibited a significant upregulation of Ser74 phosphorylation ($P < 0.01$; One-way ANOVA), whereas no detectable phosphorylation at S74 was observed in *C. gigas* after heat stress (Fig. 3A). Subsequently, we purified *Cg*IκBα protein *in vitro* for DSF experiments to investigate the impact of phosphorylation at the S74 site on protein stability. The DSF results demonstrated that the simulation of dephosphorylation at S74 significantly increased

(See figure on next page.)

Fig. 3 The function of phosphorylation at Ser74 of *Cg*IκBα. **A** The phosphorylation levels of Ser74 site of *Cg*IκBα in gill tissues of *C. gigas* and *C. angulata* during heat stress, which was obtained from our previous study [14]. **B** Thermal stabilization of *Cg*IκBα and *Cg*IκBα^{S74A} proteins, as measured via differential scanning fluorimetry (DSF). Mean Tm values ± S.D. is shown ($n = 3$). $^{*}p < 0.05$ by two-tailed unpaired t test. **C** The western blotting of nuclear and cytoplasmic proteins extracted from gill tissues of *C. gigas* and *C. angulata* during heat stress. The content of *Cg*REL1 and *Cg*REL2 were detected by immunoblotting with anti-*Cg*REl1/*Cg*REL2 antibody. Gi and An represent the *C. gigas* and *C. angulata* under control condition. HGi and HAn represent the *C. gigas* and *C. angulata* under heat stress. **D** The protein degradation experiments of different *Cg*IκBα mutants. **E** The protein ubiquitination experiments of different *Cg*IκBα mutants. **F** The western blotting of nuclear and cytoplasmic proteins from HEK292T cells transfected with Flag-*CgIκBα*/Flag-*CgIκBα*^{S74A}/Flag-*CgIκBα*^{S74D} and Myc-*CgRel1*/Myc-*CgRel2* under control and heat treatment. **G** The relative dual-luciferase reporter (DLR) values of HEK293T cells transfected with pNF-κB-Luc, pRL-TK, Myc-*CgRel1*/Myc-*CgRel2* and Flag-*CgIκBα*/Flag-*CgIκBα*^{S74A}/Flag-*CgIκBα*^{S74D}/Flag-*CgIκBα*^{S32AS36A}/Flag-*CgIκBα*$^{S32AS3A6\ S74A}$/Flag-*CgIκBα*$^{S32AS36A\ S74D}$ ($n = 3$). The error bars represent the S.D. Significant differences among groups were marked with $^{*}p < 0.05$, $^{**}p < 0.01$, $^{***}p < 0.001$, and $^{****}p < 0.0001$. "ns" indicates non-significant differences

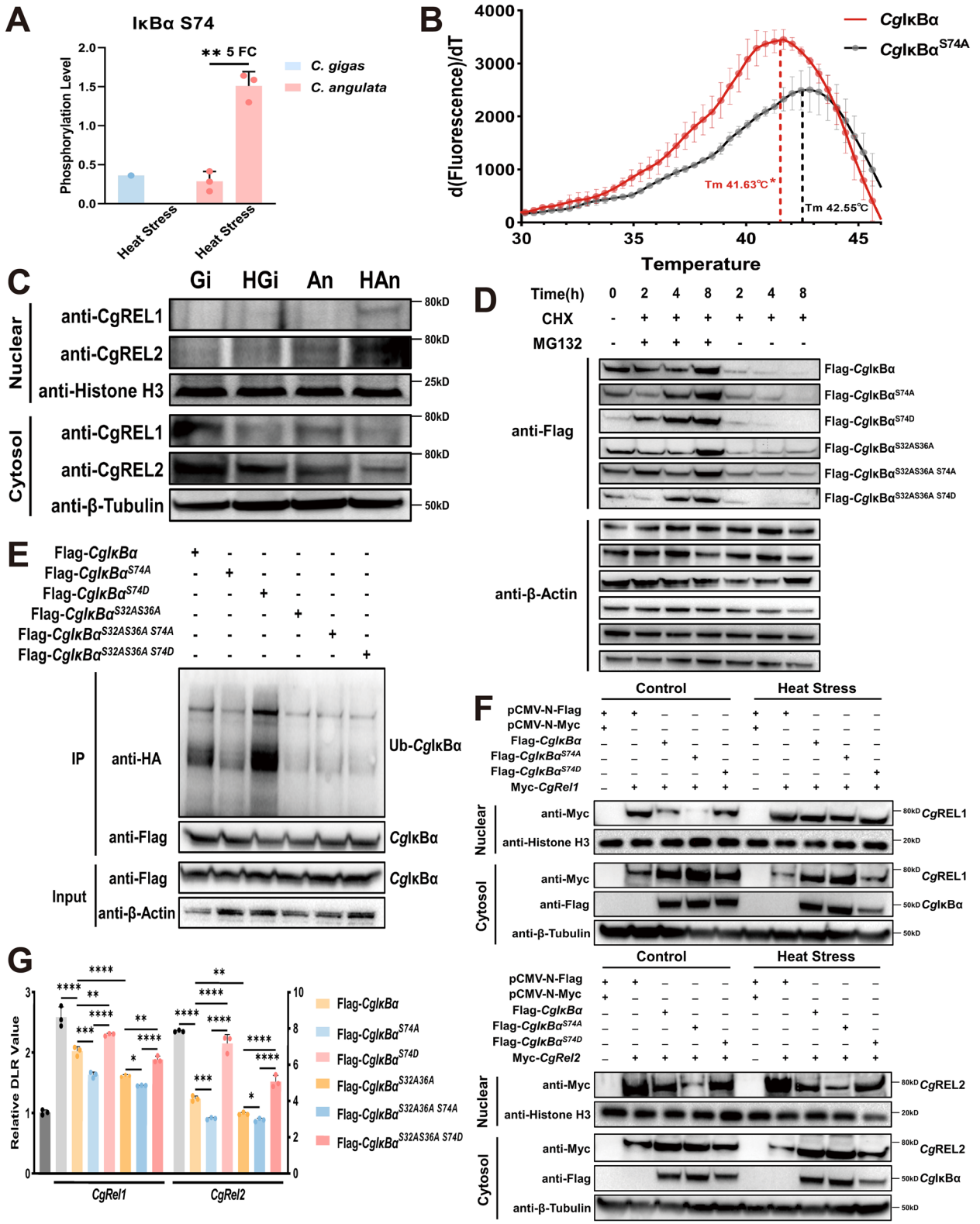

Fig. 3 (See legend on previous page.)

the thermal stability of the *Cg*IκBα protein ($P < 0.05$; two-tailed unpaired Student's t-test; Fig. 3B). Furthermore, we conducted Western blotting experiments on *C. gigas* and *C. angulata* gill tissues under heat stress to determine whether phosphorylation at the S74 site affects *Cg*IκBα ubiquitination degradation and its mediation of REL nuclear translocation in response to heat. *Crassostrea angulata* with high S74 phosphorylation levels exhibited a higher abundance of nuclear REL protein after heat stress (Fig. 3C).

Subsequently, we further refined the evaluation of the effect of S74 phosphorylation on *Cg*IκBα ubiquitination degradation based on single site mutations and co-transfection in human cells. The site mutation protein degradation experiments demonstrated substantial inhibition of ubiquitination and degradation of the *Cg*IκBα protein when treated with a combination of MG132 and CHX. When treated with CHX alone, the *Cg*IκBα^{S74D} mutant (mimicking phosphorylation)/*Cg*IκBα^{S74A} mutant (mimicking dephosphorylation) exerted an augmenting/inhibitory effect on *Cg*IκBα degradation. This effect was observed to be independent of phosphorylation at S32 and S36 (Fig. 3D). Furthermore, the protein ubiquitination experiments results were consistent with the aforementioned findings, demonstrating that phosphorylation at S74 significantly enhanced the ubiquitination level of the *Cg*IκBα protein (Fig. 3E). Western blotting showed that phosphorylation at the S74 may enhance the heat-induced nuclear translocation of *Cg*REL1 and *Cg*REL2 by promoting ubiquitination degradation of *Cg*IκBα (Fig. 3F). The luciferase reporter gene experiments further confirmed that phosphorylation of *Cg*IκBα at S74 promoted its degradation independent of S32 and S36, relieving the inhibition of *Cg*REL and enhancing its transcriptional activity in activating the NF-κB signaling pathway promoter (Fig. 3G). In addition, the cellular heat-induced apoptosis experiments ($P < 0.001$; Two-way ANOVA; Fig. S5) and CCK-8 cell viability assays ($P < 0.01$; Two-way ANOVA; Fig. S6) indicated that phosphorylation of *Cg*IκBα at the S74 site enhanced the role of *Cg*REL in thermotolerance by promoting its ubiquitin-mediated degradation.

Differential phosphorylation of *Cg*IκBα^{S74} activated cell survival-related genes to mediate divergent heat response

DAP-Seq was performed to obtain the downstream genes regulated by *Cg*REL1 and *Cg*REL2. Based on peak calling results from MACS2 software, 6,208 and 8,195 peaks ($q < 0.05$) were identified in CgREL1 and CgREL2, with an average length of 482 and 482 bp, respectively. The results of quality control and alignment of DAP-Seq were shown in Fig. S7 and Fig. S8. We screened the peaks localized within the promoter regions of genes and identified 349, 570, and 135 potential genes regulated by *Cg*REL1, *Cg*REL2, and *Cg*REL1 and *Cg*REL2, respectively (Table S7). The transcriptomic data following the RNAi experiment showed an average of 30,633,206 high-quality 150-bp paired-end reads mapped to the *C. gigas* genome, with mapping rates of 71.83% (Table S8). Principal component analysis showed that three groups exhibited complete separation, indicating the robustness of the RNAi knockdown (Fig. S9; Table S9). By integrating DAP-Seq and transcriptomic data after the RNAi experiment, along with existing gene function studies, we manually identified 69 potential target genes regulated by *Cg*REL involved in heat response (Fig. 4A). These genes exhibited DAP-Seq peaks within their promoter regions and demonstrated differential expression levels between *Cg*Rel1-siRNA/*Cg*Rel2-siRNA and control groups (Table S10). Furthermore, by incorporating previous transcriptomic data from *C. gigas* and *C. angulata* under heat stress, 26 genes were identified as differentially activated during the heat stress responses between these species (Table S10). Additionally, using previous ATAC-Seq data from *C. gigas* and *C. angulata* under heat stress, ATAC-Seq peak signals were collected from the *Cg*REL binding regions in the promoters of the above 26 genes. The results showed that 14 genes were identified with significantly higher ATAC-Seq signals in heat-stressed *C. angulata* than in *C. gigas* (Fig. 4B). Among them, two (including tyrosine-protein kinase Abl (*Abl*)) were co-regulated by *Cg*REL1 and *Cg*REL2, whereas five (such as medium-chain specific acyl-CoA dehydrogenase, mitochondrial (*Acadm*)) were specifically regulated by *Cg*REL1 and seven were

(See figure on next page.)

Fig. 4 The downstream genes differentially regulated by *Cg*REL during heat stress in *C. gigas* and *C. angulata*. **A** The heatmap of *Cg*REL-regulated downstream genes normalized expression (row) from transcriptomic data of RNAi experiment and *C. gigas* and *C. angulata* during heat stress [68]. The relative expression of each gene is indicated by color (from green, low to pink, high). **B** The values of ATAC-Seq signal in the *Cg*REL binding regions within promoter of *Cg*REL-regulated downstream genes from *C. gigas* and *C. angulata* under heat stress [68]. **C** The relative dual-luciferase reporter (DLR) values of cells co-transfected with the promoter of the *Abl*/*Eif1b*/*Elovl6*/*Acadm*/*Gst*/*Map2k6* or their corresponding *Cg*REL binding region deletion mutations ligated with pGL3-basic plasmid, and Myc-*CgRel1*/Myc-*CgRel2* ($n = 3$). The error bars represent the S.D. Significant differences among groups were marked with $^{*}p < 0.05$, $^{**}p < 0.01$, $^{***}p < 0.001$, and $^{****}p < 0.0001$. "ns" indicates non-significant differences

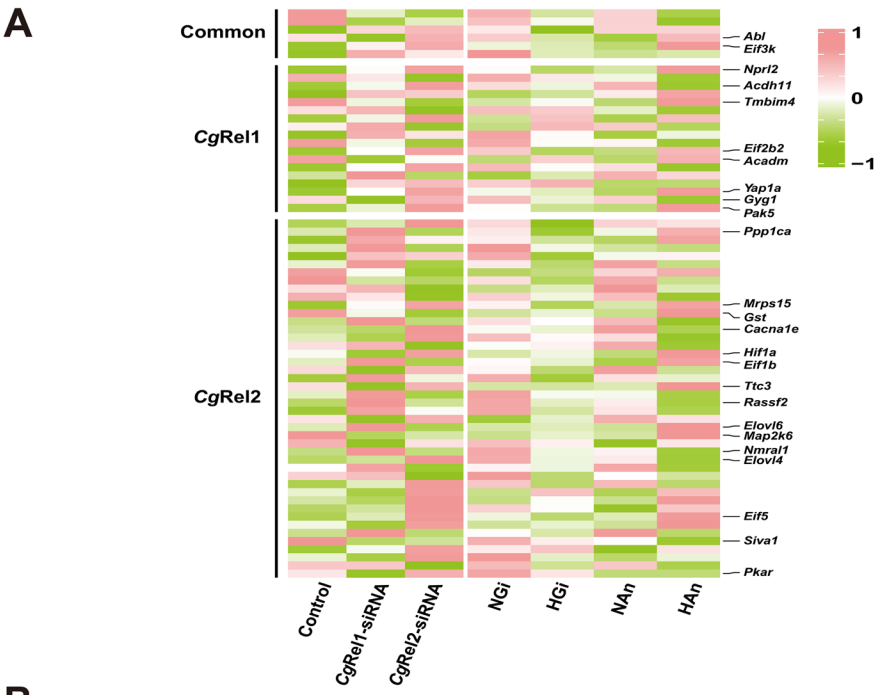

B

	Gene ID	Gene Name	Position			ATAC-Seq Signal				HGi/NGi		HAn/NAn		NAn/NGi		HAn/HGi	
			Chr	Start	End	NGi	HGi	NAn	HAn	Ratio	*p*-value	Ratio	*p*-value	Ratio	*p*-value	Ratio	*p*-value
Common	Cg15220	*Abl*	CHR05	36362442	36362851	37.4	35.0	57.0	56.4	0.93	0.7511	0.99	0.9552	1.52	0.1890	1.61	0.0049
	Cg27412	*Eif3k*	CHR09	30208164	30208564	34.6	26.8	58.1	42.4	0.77	0.2642	0.73	0.3199	1.68	0.1731	1.58	0.0411
CgRel1	Cg03966	*Nprl2*	CHR02	7970859	7971363	45.0	32.6	43.2	44.5	0.72	0.0313	1.03	0.8473	0.96	0.8128	1.37	0.0092
	Cg07273	*Acds11*	CHR02	61064715	61064982	55.4	37.2	39.3	54.5	0.67	0.1371	1.39	0.2410	0.71	0.3245	1.47	0.0095
	Cg10480	*Tmbim4*	CHR04	9534232	9534743	26.1	31.2	28.6	29.9	1.19	0.1927	1.04	0.8318	1.10	0.6578	0.96	0.7264
	Cg17412	*Mcu*	CHR06	12447266	12447635	61.3	45.2	70.0	61.3	0.74	0.3001	0.88	0.4979	1.14	0.6089	1.36	0.1382
	Cg17550	*Eif2b2*	CHR06	14870514	14871171	16.1	15.9	34.5	25.3	0.99	0.9046	0.73	0.2703	2.14	0.0173	1.59	0.1744
	Cg20410	*Acadm*	CHR07	7997266	7997886	26.0	29.5	22.5	35.8	1.13	0.7744	1.59	0.0360	0.86	0.7807	1.21	0.0341
	Cg23730	*Yap1a*	CHR08	13067890	13068304	70.6	81.2	87.1	109.8	1.15	0.4379	1.26	0.0349	1.23	0.2337	1.35	0.0237
	Cg24837	*Gyg1*	CHR08	32104590	32105157	38.1	35.8	53.5	45.2	0.94	0.5822	0.84	0.0513	1.40	0.0283	1.26	0.0063
	Cg25937	*Pak5*	CHR09	7300611	7300853	53.4	44.5	52.5	36.9	0.83	0.6849	0.70	0.5823	0.98	0.9759	0.83	0.6752
CgRel2	Cg05531	*Ppp1ca*	CHR02	31752553	31752835	27.3	8.2	30.5	28.3	0.30	0.1332	0.93	0.8904	1.12	0.8515	3.45	0.0610
	Cg09926	*Mrps15*	CHR03	58797914	58798283	52.7	30.9	38.8	44.9	0.59	0.1073	1.16	0.5670	0.74	0.3654	1.45	0.0418
	Cg11102	*Gst8*	CHR04	24361222	24361675	44.2	33.3	39.5	50.2	0.75	0.0864	1.27	0.0479	0.89	0.3623	1.51	0.0143
	Cg13452	*Cacna1e*	CHR05	6959435	6960178	63.9	39.3	47.5	29.7	0.62	0.0696	0.63	0.1035	0.74	0.1969	0.76	0.2805
	Cg15346	*Hif1a*	CHR05	38261382	38261786	108.7	96.1	115.2	92.7	0.88	0.7085	0.80	0.4442	1.06	0.8528	0.96	0.8976
	Cg15547	*Eif1b*	CHR05	41124502	41124788	27.0	11.1	59.4	35.1	0.41	0.2388	0.59	0.3127	2.20	0.2258	3.17	0.0383
	Cg16417	*Ttc3*	CHR05	56277224	56277510	48.1	44.5	62.7	71.5	0.92	0.5801	1.14	0.2829	1.30	0.0668	1.61	0.0209
	Cg17496	*Rassf4*	CHR06	14086842	14087170	5.3	5.3	5.0	3.8	1.01	0.9904	0.75	0.5012	0.96	0.9540	0.71	0.0891
	Cg19506	*Elovl6*	CHR06	49477333	49477616	24.0	28.2	38.7	53.3	1.18	0.3336	1.38	0.0637	1.61	0.0814	1.89	0.0008
	Cg19595	*Map2k6*	CHR06	50979657	50980123	51.2	38.9	51.6	46.1	0.76	0.4210	0.89	0.6004	1.01	0.9839	1.19	0.0101
	Cg21261	*Nmral1*	CHR07	23805094	23805433	57.2	40.9	44.0	31.5	0.72	0.0030	0.72	0.1777	0.77	0.1463	0.77	0.0493
	Cg21326	*Elovl4*	CHR07	25209237	25209633	12.9	8.6	8.1	14.8	0.67	0.3502	1.84	0.1385	0.62	0.3002	1.71	0.1620
	Cg26856	*Eif5*	CHR09	18745271	18745658	17.2	21.5	29.5	22.6	1.25	0.4474	0.77	0.0581	1.71	0.0011	1.05	0.8476
	Cg28473	*Siva1*	CHR09	47652288	47652646	33.1	19.7	22.5	22.1	0.59	0.1142	0.98	0.9203	0.68	0.2186	1.12	0.3652
	Cg29595	*Pkar*	CHR10	13332608	13332879	49.5	31.4	44.7	52.9	0.63	0.1106	1.18	0.5159	0.90	0.6463	1.68	0.1181

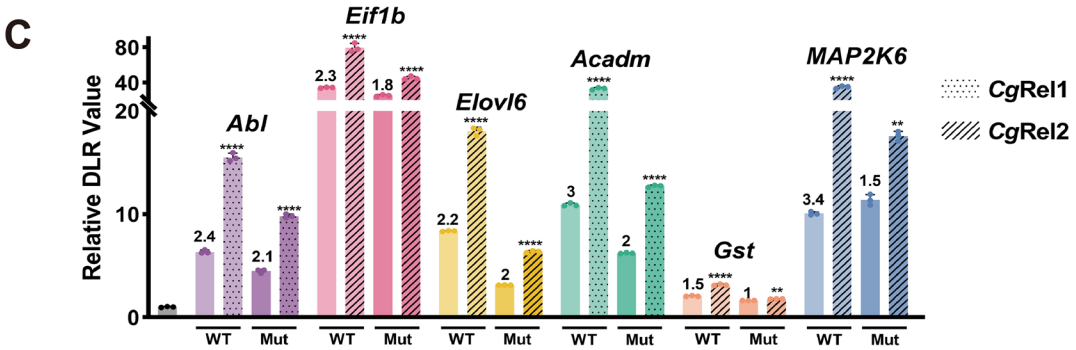

Fig. 4 (See legend on previous page.)

specifically regulated by *Cg*REL2 (such as glutathione S-transferase 8 (*Gst*)).

Subsequently, we amplified the promoter regions of above genes and conducted luciferase reporter assays with binding region deletion mutations and *Cg*REL co-transfection in human cells to elucidate the regulatory relationship of REL on these genes. The results showed that two (*Abl* and *Acadm*) and four (eukaryotic translation initiation factor 1 (*Eif1b*), elongation of very long chain fatty acids protein 6 (*Elovl6*), dual specificity mitogen-activated protein kinase kinase 6 (*Map2k6*), and *Gst*) genes specifically activated by *Cg*REL1 and *Cg*REL2, respectively, which exhibited lower increase in fluorescence intensity in the mutant-type transfected with *Cg*REL than the wild-type (One-way ANOVA; Fig. 4C). Using *Acadm* as an example, the REL1 binding region within its promoter region exhibited differential accessibility during heat stress in *C. gigas* and *C. angulata* (Fig. S10), suggesting that *Cg*REL1 may enhance the expression of *Acadm* in *C. angulata* under heat stress by increasing its interactions with the binding region of the promoter. Moreover, the EMSA experiment was performed to confirm the specificity of *Cg*REL1 binding to the promoter region of *Acadm*. The transfection of Myc-*CgRel1* into cellular nuclear extract caused significant retardation of band migration (lanes 1, 2, 3, 4), and the results of super shift further supported the binding specificity (Lane 5; Fig. S11). Additionally, we performed repeated validation of the ability of *Cg*IκBα S74 phosphorylation to independently mediate protein degradation using the luciferase reporter assay and *Acadm* promoter (Fig. S12).

*Cg*ERK1/2 phosphorylated *Cg*IκBα S74 to promote its ubiquitination degradation

Based on the results of kinase prediction, we identified numerous kinases associated with the MAPK pathway, with a particular emphasis on the ERK genes (Table S11). Phylogenetic analysis confirmed the identification of oyster ERK protein as ERK1/2 (Fig. 5A).

Subsequently, by co-transfecting *Cg*ERK1/2 and *Cg*IκBα in human cells, we investigated the interaction and phosphorylation modification relationship between these two proteins. The Co-IP results demonstrated the specific interaction between *Cg*ERK1/2 and *Cg*IκBα (Fig. 5B). The yeast two-hybrid (Fig. 5C) and BiFC assays (Fig. 5D) provided additional evidence supporting the specific interaction between *Cg*ERK1/2 and *Cg*IκBα, predominantly localized within the cytoplasm. The subcellular localization results demonstrated that *Cg*ERK1/2 markedly attenuated the inhibitory effect of *Cg*IκBα on *Cg*REL, consequently promoting nuclear translocation of REL proteins in response to heat stress (Fig. 5E). The *in vivo* kinase experiments (Fig. 5F) and *in vitro* kinase experiments (Fig. 5G) demonstrated the specific kinase-substrate relationship between *Cg*ERK1/2 and *Cg*IκBα Ser74 site.

Furthermore, the protein ubiquitination experiment showed that co-transfection of *Cg*ERK1/2 and *Cg*IκBα^{S32AS36A} caused a significant increase in the ubiquitination level of *Cg*IκBα, which was effectively weakened by the *Cg*IκBα$^{S32AS36A\ S74A}$ mutant (Fig. 6A). The protein degradation experiments demonstrated that *Cg*ERK1/2 significantly promoted *Cg*IκBα degradation, which was unaffected by phosphorylation at S32 and S36. The S74 dephosphorylation mutation effectively prevented the *Cg*IκBα protein degradation by blocking the ERK-mediated phosphorylation at S74 (Fig. 6B). Western blotting on heat-stress cells further confirmed that *Cg*ERK1/2 facilitated the degradation of *Cg*IκBα, enabling increased nuclear translocation of *Cg*REL1 and *Cg*REL2 during high temperatures, which was inhibited by the S74 dephosphorylation mutation (Fig. 6C). Additionally, the luciferase reporter experiments demonstrated that *Cg*ERK1/2, independent of phosphorylation at S32 and S36, can gradiently increase the activation of *Cg*REL-mediated NF-κB signaling pathway transcriptional activity (Fig. 6D). The cellular heat-induced apoptosis experiments (Fig. 6E) and the corresponding CKK-8 cell viability measurements (Fig. 6F) provided additional evidence that *Cg*ERK1/2 is crucial in mitigating

(See figure on next page.)

Fig. 5 The interaction and kinase reaction between *Cg*ERK1/2 and *Cg*IκBα. **A** Phylogenetic tree of oyster, human, mouse and zebrafish ERK gene family. The tree was constructed with the maximum likelihood (ML) method using PhyloSuite. Bootstrap support values are indicated by sizes on nodes of phylogenetic tree. The *Cg*ERK1/2 is marked with red bold line. Different colors indicate different categories of ERK subfamilies. Cg, *Crassostrea gigas*; Hm, *Homo sapiens*; Mm, *Mus musculus*; Dr, *Danio rerio*. The accession numbers were as follows: *Hm* ERK1, NP_002737.2; *Hm* ERK2, NP_002736.3; *Hm* ERK3, NP_002739.1; *Hm* ERK4, NP_002738.2; *Hm* ERK5, NP_002740.2; *Hm* ERK6, NP_002960.2; *Hm* ERK7, NP_620590.2; *Mm* ERK1, NP_036082.1; *Mm* ERK2, NP_001033752.1; *Mm* ERK3, NP_056621.4; *Mm* ERK4, NP_766220.2; *Mm* ERK5, NP_001277963.1; *Mm* ERK6, NP_001389948.1; *Mm* ERK7, NP_808590.1; *Dr* ERK1, NP_958915.1; *Dr* ERK3, NP_001039017.1; *Dr* ERK4, NP_998638.1; *Dr* ERK5, NP_001013469.2; *Dr* ERK6, NP_571482.1; *Dr* ERK7, XP_009292731.1. The sequences of *Cg*ERK1/2 (Cg03498) gene in oyster were obtained from *Crassostrea gigas* genome blast (GCA_011032805.1). **B** Co-immunoprecipitation (co-IP) of *Cg*IκBα with *Cg*ERK1/2. **C** Yeast two-hybrid assay between *Cg*IκBα and *Cg*ERK1/2. **D** BiFC assay of *Cg*IκBα and *Cg*ERK1/2. Bar: 10 μm. **E** Subcellular localization of *Cg*IκBα, *Cg*REL and *Cg*ERK1/2 in HeLa cells under control and heat stress. Bar: 10 μm. **F** *In vivo* phosphorylation assay of *Cg*ERK1/2 on *Cg*IκBα Ser74 site. **G** *In vitro* kinase activity assay of *Cg*ERK1/2 on *Cg*IκBα Ser74 site. CBB, Coomassie Brilliant Blue staining

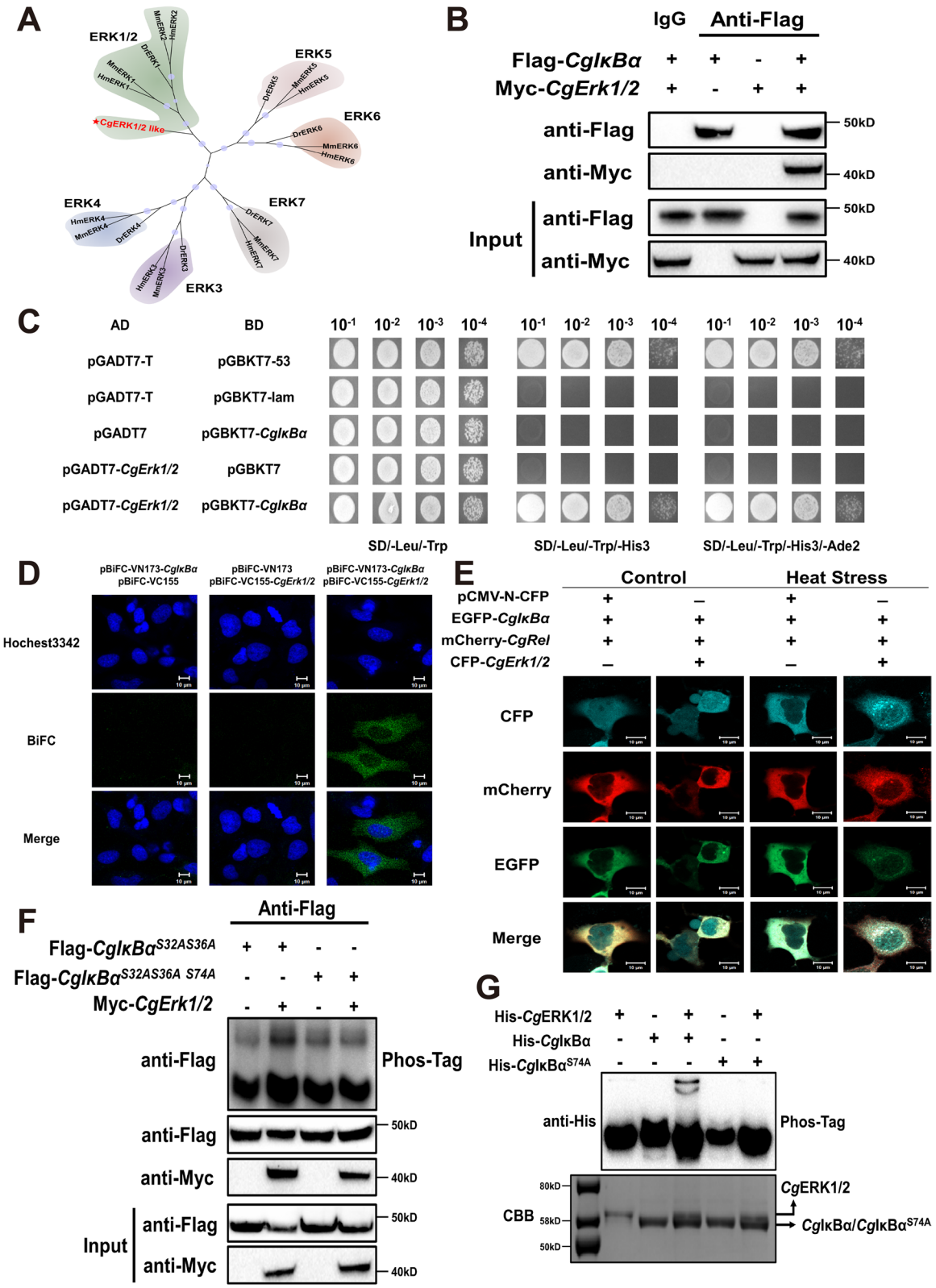

Fig. 5 (See legend on previous page.)

the inhibitory effect of *Cg*IκBα on *Cg*REL1 and *Cg*REL2, and enhanced *Cg*REL's role in facilitating cell resistance against high-temperature-induced cell death.

Divergent phosphorylation of *Cg*ERK1/2$^{T187\ Y189}$ regulated by MAPK pathway mediated differential NF-κB pathway activity

The sequence alignment results showed that the oyster ERK1/2 residues T187 and Y189 correspond to the conserved active sites T202 and Y204, respectively, in human ERK1 (Fig. 7A). Previous phosphoproteomic data from *C. gigas* and *C. angulata* during heat stress revealed distinct patterns of phosphorylation at the *Cg*ERK1/2 T187 and Y189 sites. The phosphorylation level at the *Cg*ERK1/2 T187 site increased in *C. angulata* and decreased in *C. gigas* and significantly increased at the *Cg*ERK1/2 Y189 site only in *C. angulata* under heat stress ($P < 0.05$; Fig. 7B).

Then, we co-transfected *Cg*ERK1/2 phosphorylation mutants and *Cg*IκBα in human cells to investigate whether differential phosphorylation of *Cg*ERK1/2 in response to heat affects *Cg*IκBα ubiquitination degradation. *In vivo* (Fig. 5C) and *in vitro* (Fig. 5D) kinase assays, coupled with *Cg*ERK1/2$^{T187D\ Y189E}$ (mimicking phosphorylation) and *Cg*ERK1/2$^{T187A\ Y189F}$ (mimicking dephosphorylation) mutants provided compelling evidence that phosphorylation at *Cg*ERK1/2 T187 and Y189 significantly enhanced its kinase activity, causing an elevated phosphorylation level of *Cg*IκBα S74 site. In addition, the protein ubiquitination experiments showed that phosphorylation at *Cg*ERK1/2 T187 and Y189 significantly enhanced the ubiquitination level of *Cg*IκBα$^{S32A\ S36A}$ (Fig. 7E). Western blotting on heat-stress cells further demonstrated that phosphorylation at *Cg*ERK1/2 T187 and Y189 contributed to the enhancement of its kinase activity, promoting *Cg*IκBα degradation to facilitate the nuclear translocation of *Cg*REL1 and *Cg*REL2 in response to heat stress (Fig. 7F). Similarly, the *Cg*ERK1/2 T187 and Y189 phosphorylation mutants significantly enhanced REL-mediated positive transcriptional activity in the NF-κB signaling pathway ($P < 0.05$; One-way ANOVA; Fig. 7G). Furthermore, the cellular heat-induced apoptosis experiments (Fig. S13) and CCK-8 cell viability measurements (Fig. S14) provide additional evidence supporting the role of *Cg*ERK1/2 T187 and Y189 phosphorylation in facilitating *Cg*IκBα^{S32AS36A} degradation and amplifying the protective effect of *Cg*REL against heat stress-induced cell death.

To further assess the activation status of the MAPK/ERK pathway, we conducted Western blotting analysis on *C. gigas* and *C. angulata* under heat stress. The results demonstrated that *Cg*ERK1/2 phosphorylation levels were clearly higher in *C. angulata* than in *C. gigas* (Fig. 8A). Based on genome annotation and phylogenetic analysis, one Braf- and three Ras-like genes were found in oysters (Fig. S15A). Among them, the Ras-like genes were clustered into three subfamilies, including Mras, Rras2, and Ras-like. *CgRras2*- and *CgRas*-like genes showed no response to heat stress, except *CgMras* (Fig. S15B). The upstream regulators of ERK, including the phosphorylation level of MAP2K1/2 like (Fig. S16; Fig. 8A), relative expression of *Braf* ($P < 0.01$; Two-way ANOVA; Fig. 8B) and *Mras* ($P < 0.001$; Two-way ANOVA; Fig. 8B), and protein content of MAP3K1 (Fig. 8A) were significantly higher in HAn (*C. angulata* after heat stress) than in HGi (*C. gigas* after heat stress).

Additionally, we further confirmed the activating effect of the upstream regulator *Cg*MAP2K1/2 in the MAPK pathway on the *Cg*ERK1/2-*Cg*IκBα-*Cg*REL cascade signaling pathway by co-transfecting human cells. The *in vivo* kinase experiment (Fig. 8C) and ubiquitination assay (Fig. 8D) proved that *Cg*MAP2K1/2 can increase the phosphorylation and ubiquitination levels of *Cg*IκBα$^{S32A\ S36A}$ by phosphorylating *Cg*ERK1/2. Similarly, co-transfection of *Cg*MAP2K1/2 and *Cg*ERK1/2 caused an increased nuclear translocation of *Cg*REL in response to heat stress (Fig. 8E), significantly reducing cellular heat-induced apoptosis rate ($P < 0.0001$; Two-way ANOVA; Fig. S17A, S17B) and promoting cell viability ($P < 0.0001$; Two-way ANOVA; Fig. S17C, S17D). Furthermore, the luciferase reporter experiments confirmed

(See figure on next page.)

Fig. 6 *Cg*ERK1/2 phosphorylates *Cg*IκBα S74 to promote its Ubiquitination degradation. **A** The protein ubiquitination experiments of *Cg*IκBα^{S32AS36A}/*Cg*IκBα$^{S32AS36A\ S74A}$ co-transfected with CgERK1/2. **B** The protein degradation experiments of *Cg*IκBα/*Cg*IκBα^{S74A}/*Cg*IκBα^{S32AS36A}/*Cg*IκBα$^{S32AS36A\ S74A}$ co-transfected with CgERK1/2. **C** The western blotting of nuclear and cytoplasmic proteins from HEK292T cells transfected with Flag-*CgIκBα*/Flag-*CgIκBα*^{S74A}, Myc-*CgRel1*/Myc-*CgRel2* and Myc-*CgErk1/2* under control and heat treatment. **D** The relative dual-luciferase reporter (DLR) values of HEK293T cells transfected with pNF-κB-Luc, pRL-TK, Myc-*CgRel1*/Myc-*CgRel2*, Flag-*CgIκBα*/Flag-*CgIκBα*^{S74A}/Flag-*CgIκBα*^{S32AS36A}/Flag-*CgIκBα*$^{S32AS36A\ S74A}$ and Myc-*CgErk1/2* ($n = 3$). Among these, the transfection amounts of Myc-*CgErk1/2* was increased in a gradient manner, with doses of 100 ng, 200 ng, 300 ng, and 400 ng per well of a 24-well plate, respectively. The cell apoptosis rate (**E**; $n = 3$) and the CCK-8 assay for the cell viability (**F**; $n = 5$) of HEK293T cells transfected with Flag-*CgIκBα*^{S32AS36A}/Flag-*CgIκBα*$^{S32AS36A\ S74A}$, Myc-*CgRel1*/Myc-*CgRel2* and Myc-*CgErk1/2* under control and heat treatment ($n = 3$). The left panel is the cell apoptosis chart in each group, and the right panel is the cell apoptosis rate in each group. The error bars represent the S.D. Significant differences among groups were marked with $^{*}p < 0.05$, $^{**}p < 0.01$, $^{***}p < 0.001$, and $^{****}p < 0.0001$. "ns" indicates non-significant differences

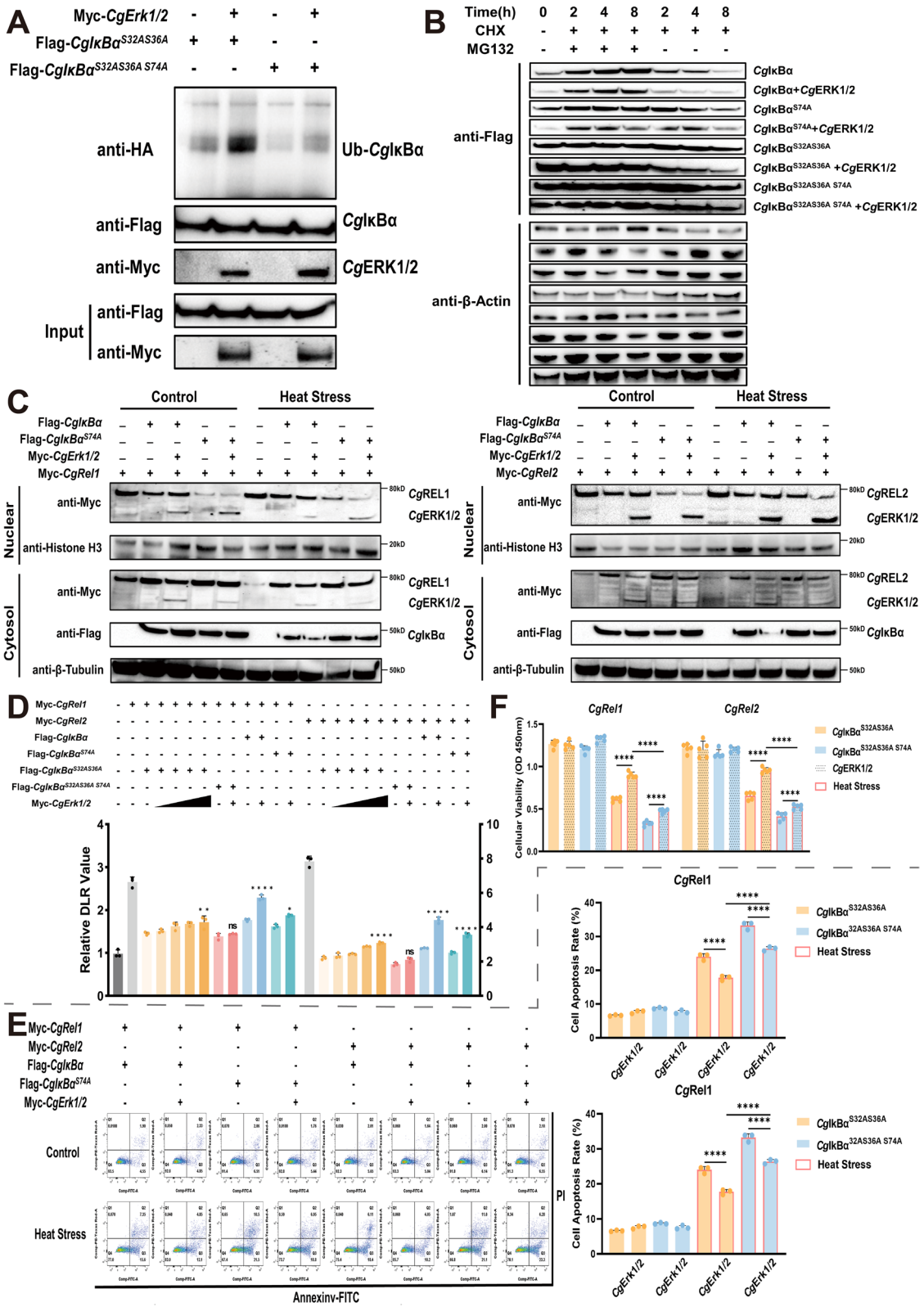

Fig. 6 (See legend on previous page.)

that *Cg*MAP2K1/2 could enhance *Cg*ERK1/2 kinase activity through phosphorylation, promoting *Cg*IκBα$^{S32A\ S36A}$ degradation and significantly increasing *Cg*REL-mediated transcriptional activity in the NF-κB signaling pathway ($P < 0.001$; Fig. 8F).

Oyster's MAPK/ERK/IκBα/REL regulatory *axis* exhibited environmental responsiveness

The 8-month-old F_1 progeny of *C. gigas* and *C. angulata* were transplanted into their native and nonnative habitats, the northern (Qingdao, 35°44′ N) and southern (Xiamen, 24°33′ N) regions of China, and their corresponding protein phosphorylation and gene expression levels were evaluated after a 3-month reciprocal transplantation between local and non-local environments (Fig. S18). The average seawater temperature in the southern habitat (19.64℃) was significantly higher than that in the northern habitat (11.24℃; $P < 0.0001$, Fig. 9A), reflecting the distinct environmental temperature variations between the natural habitats of the two species. Western blotting of reciprocally-transplanted *C. gigas* and *C. angulata* demonstrated that the protein levels of *Cg*ERK1/2 and *Cg*MAP2K1/2 remained unaffected by the environment. However, their phosphorylation levels (*Cg*ERK1/2$^{T187\ Y189}$ (corresponding to *Hm*ERK1$^{T202\ Y204}$) and *Cg*MAP2K1/2^{S238} (corresponding to *Hm*MAP2K1^{S218})) showed a divergent pattern, with higher levels observed in the southern habitat than the northern habitat and in *C. angulata* than in *C. gigas* (Fig. 9B). Moreover, the protein content of CgMAP3K1 and gene expression levels of *CgBraf* and *CgMras* demonstrated a similar trend (Fig. 9C). Furthermore, the REL-mediated downstream genes, including *Abl*, *Elovl6*, *Acadm*, *Eif1b*, *Gst*, and *Map2k6* displayed the same expression pattern (Fig. 9D).

Discussion

The NF-κB signaling pathway, widely recognized as a conserved signaling pathway, has been extensively shown to be crucial in the biological immune processes of vertebrates and invertebrates [15–17, 24, 25, 32]. In this study, the phylogenetic analysis and sequence alignment identified three or four IκBα proteins in oysters, and most IκBα proteins in mollusks exhibit conserved Ser32 and Ser36 sites, consistent with the findings of previous studies [25, 26, 37]. Notably, our previous study identified a novel heat-induced phosphorylation site (Ser74) in the IκB protein of oysters [14]. Of particular interest in this study is the *Cg*IκB like4 protein (*Cg*IκBα), which displayed the highest expression level among four IκBα proteins in *C. gigas* and possessed a specifically evolved Ser74 site in oysters. *Cg*IκBα demonstrated a response to high temperature and other abiotic stresses. Moreover, an opposite phosphorylation pattern at S74 (upregulated in *C. angulata* and downregulated in *C. gigas*) was observed between *C. gigas* (relatively low temperature adapted species) and *C. angulata* (relatively high temperature adapted species) during heat stress, whereas no phosphorylation modifications were detected at S32 and S36 [14]. Further functional experiments focusing on the phosphorylation of the *Cg*IκBα at the S74 site demonstrated that phosphorylation at this site can independently facilitate *Cg*IκBα degradation through the ubiquitin–proteasome pathway, which differs from the established mechanism in model organisms where phosphorylation at Ser32 and Ser36 sites by IKKs primarily controls the degradation of IκBα protein [22, 23]. Additionally, the DSF results revealed that the phosphorylation at Ser74 of *Cg*IκBα significantly reduces its thermal stability, further proving that the decreased stabilization induced by phosphorylation can increase the ubiquitination level similar to p53 phosphorylation by aurora kinase A [69]. Therefore, we propose that heat-induced novel phosphorylation at Ser74 of *Cg*IκBα can aid oysters in combating thermal stress by activating the NF-κB pathway through reduced thermal stabilization and increased ubiquitination and that its divergent heat response patterns in the two congenic oysters suggest its significant role in temperature adaptation. However, owing to the insufficient phosphoproteomics data in mollusks, we cannot determine

(See figure on next page.)

Fig. 7 The divergent phosphorylation pattern of ERK regulates differential phosphorylation level of Ser74 site at *Cg*IκBα between *C. gigas* and *C. angulata* during heat stress. **A** The sequence alignment of human ERK1, ERK2 and oyster ERK1/2. Different colors of sequence correspond to the degree of amino acid conservation (from light blue, low to blue, high). And the lower ribbon of sequence indicates different active sites or domain. Arrow marks the sequence alignment surrounding T187 and Y189 on *Cg*ERK1/2 protein. **B** The phosphorylation levels of Thr187 and Tyr189 sites of *Cg*ERK1/2 in gill tissues of *C. gigas* and *C. angulata* during heat stress, which was obtained from our previous study [14]. **C** *In vivo* phosphorylation assay of different *Cg*ERK1/2 mutants on *Cg*IκBα Ser74 site. **D** *In vitro* kinase activity assay of *Cg*ERK1/2/CgERK1/2^{T187AY189F} on *Cg*IκBα Ser74 site. CBB, Coomassie Brilliant Blue staining. **E** The protein ubiquitination experiments of *Cg*IκBα^{S32AS36A} co-transfected with *Cg*ERK1/2/*Cg*ERK1/2^{T187AY189F}/*Cg*ERK1/2^{T187DY189E}. **F** The western blotting of nuclear and cytoplasmic proteins from HEK292T cells transfected with Flag-*CgIκBa*^{S32AS36A}, Myc-*CgErk1/2*/Myc-*CgErk1/2*^{T187AY189F}/Myc-*CgErk1/2*^{T187DY189E} and Myc-*CgRel1*/Myc-*CgRel2* under control and heat treatment. **G** The relative dual-luciferase reporter (DLR) values of HEK293T cells transfected with pNF-κB-Luc, pRL-TK, Myc-*CgRel1*/Myc-*CgRel2*, Flag-*CgIκBa*^{S32AS36A}/Flag-*CgIκBa*$^{S32AS36A\ S74A}$ and Myc-*CgErk1/2*/Myc-*CgErk1/2*^{T187AY189F}/Myc-*CgErk1/2*^{T187DY189E} ($n = 3$). The error bars represent the S.D. Significant differences among groups were marked with $^{*}p < 0.05$, $^{**}p < 0.01$, $^{***}p < 0.001$, and $^{****}p < 0.0001$. "ns" indicates non-significant differences

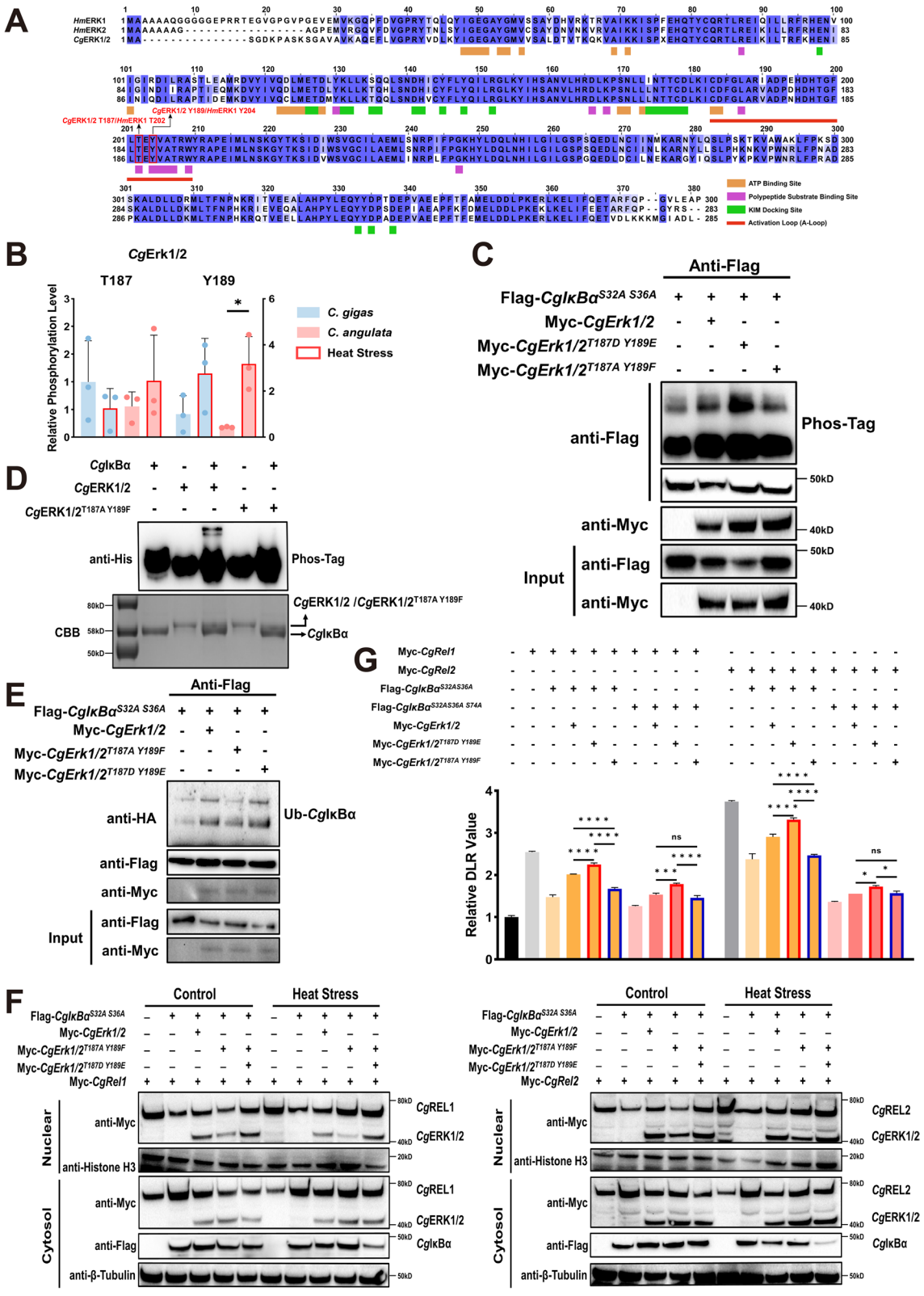

Fig. 7 (See legend on previous page.)

whether phosphorylation at the Ser74 of *Cg*IκBα in oysters responds to other non-biological stressors.

Based on kinase prediction and subsequent functional validation, we confirmed that the MAPK/*Cg*ERK1/2 kinase phosphorylated Ser74 site of *Cg*IκBα, then activated the NF-κB/REL pathway to resist heat stress. ERK1 and ERK2 belong to the highly conserved MAPK family and phosphorylate many substrates, regulating a variety of evolutionarily conserved cellular processes in metazoans [70]. Previous studies on the signal crosstalk between MAPK/ERK and NF-κB/IκBα pathways have found a significant association (positive [71–75] or negative [76, 77]) between the phosphorylation levels of ERK and IκBα, which are usually mediated through IKKs. However, our study first reported a direct kinase-substrate interaction between MAPK/ERK and NF-κB/IκBα proteins in oysters exposed to high-temperature, which bypasses the known IκBα upstream kinase IKKs and does not rely on the Ser32 and Ser36 sites. Further measurements of phosphorylation and expression levels in key kinases and regulatory factors of the classical MAPK pathway showed that *C. angulata* demonstrated a stronger activation pattern in classical MAPK pathway than *C. gigas* during heat stress and under increased wild environmental temperature, as evidenced by higher phosphorylation levels of *Cg*ERK1/2 at T187 and Y189 and *Cg*MAP2K1/2 at S238 and S242, the protein content of MAP3K1, and the expression levels of *CgBraf* and *CgMras*. MAPK/ERK pathway reportedly participates in the high-temperature stress response in marine invertebrates [11, 78–81] and other taxa, activating the expression of heat shock proteins [82, 83], mitigating oxidative stress and mitochondrial damage [84, 85], and ultimately promoting cell survival and inhibiting apoptosis [86]. The co-transfection of *Cg*MAP2K1/2 and *Cg*ERK1/2 demonstrated that activated *Cg*ERK1/2 can further upregulate the phosphorylation at the S74 site of *Cg*IκBα protein and subsequent degradation, increasing the transcriptional activity of *Cg*REL. According to the existing classical MAPK pathway, the activation of ERK1/ERK2 is achieved through the phosphorylation of Thr-202/185 and Tyr-204/187 sites by MAP2K1/MAP2K2 [87], the Ser-218/222 and Ser-222/226 sites of MAP2K1/MAP2K2 are phosphorylated by RAF or MAP3K1 [88], and the RAF is activated by Ras-GTP through membrane recruitment and other kinases (such as PKA, PAK, and SRC) [89]. Among RAS family, the MRAS exhibited high-temperature responsiveness in this study and is reportedly crucial in enhancing MAPK signal transduction by counteracting inhibitory phosphorylation events on the RAF protein family through SHOC2-MRAS-PP1C complex [90]. Additionally, there is evidence suggesting that RAS can be activated by the receptor tyrosine kinase (RTK) to regulate cell proliferation and survival through the downstream MAPK cascade during heat stress, similar to those induced by growth factor stimulation [91]. Our previous study revealed significant differences in the protein content and phosphorylation modifications of RTKs, such as FGFR3, during the thermal stress between *C. gigas* and *C. angulata* [14]. Our results indicate that the presence of a high-temperature-RTK-MRAS-BRAF-MAPK-NF-κB signaling cascade in oysters, with the core components being the activation of MAPK/ERK and the phosphorylation of its substrate IκBα (Ser74), followed by ubiquitin-mediated proteasomal degradation, which exhibits inter-species differentiation and responses to elevated environmental temperatures, and is essential in shaping the divergent temperature adaptation.

The function experiments had proven that NF-κB/*Cg*IκBα interact with *Cg*REL1 and *Cg*REL2 in the cytoplasm, suppressing its nuclear translocation and transcriptional activity, which are consistent with previous reports on the other three *Cg*IκBα proteins [25, 37, 92]. Subsequent investigations had revealed that *Cg*REL possessed a high-temperature nuclear translocation capability, which is crucial in cellular and oysters' defenses against cell death induced by heat stress. This is consistent with the findings by Liu et al. that the levels of RelA (p65) and phosphorylation of IκBα in chickens subjected to high temperature significantly increased, supporting the involvement of NF-κB/Rel pathway in the response to heat stress [93].

(See figure on next page.)

Fig. 8 The MAPK/ERK signaling pathway regulates the phosphorylation level of Ser74 site at *Cg*IκBα. **A** The western blotting of proteins extracted from gill tissues of *C. gigas* and *C. angulata* during heat stress with MAPK pathway's antibodies. Gi and An represent the *C. gigas* and *C. angulata* under control condition. HGi and HAn represent the *C. gigas* and *C. angulata* under heat stress. **B** The expressions of *CgBraf* and *CgMras* from transcriptomic data of *C. gigas* and *C. angulata* during heat stress ($n = 3$) [68]. **C** *In vivo* phosphorylation assay of *Cg*IκBα^{S32AS36A} co-transfected with *Cg*ERK1/2/*Cg*ERK1/2^{T187AY189F} and *Cg*MAP2K1/2. **D** The protein ubiquitination experiments of *Cg*IκBα^{S32AS36A} co-transfected with *Cg*ERK1/2/*Cg*ERK1/2^{T187AY189F} and *Cg*MAP2K1/2. **E** The western blotting of nuclear and cytoplasmic proteins of HEK293T cells transfected with Flag-*CgIκBα*^{S32AS36A}, Myc-*CgRel1*/Myc-*CgRel2*, Myc-*CgErk1/2*/Myc-*CgErk1/2*^{T187AY189F} and His-*CgMap2k1/2* under control and heat treatment. **F** The relative dual-luciferase reporter (DLR) values of HEK293T cells transfected with pNF-κB-Luc, pRL-TK, Myc-*CgRel1*/Myc-*CgRel2*, Flag-*CgIκBα*^{S32AS36A}, Myc-*CgErk1/2*/Myc-*CgErk1/2*^{T187AY189F} and His-*CgMap2k1/2* ($n = 3$). The error bars represent the S.D. Significant differences among groups were marked with $^{*}p < 0.05$, $^{**}p < 0.01$, $^{***}p < 0.001$, and $^{****}p < 0.0001$. "ns" indicates non-significant differences

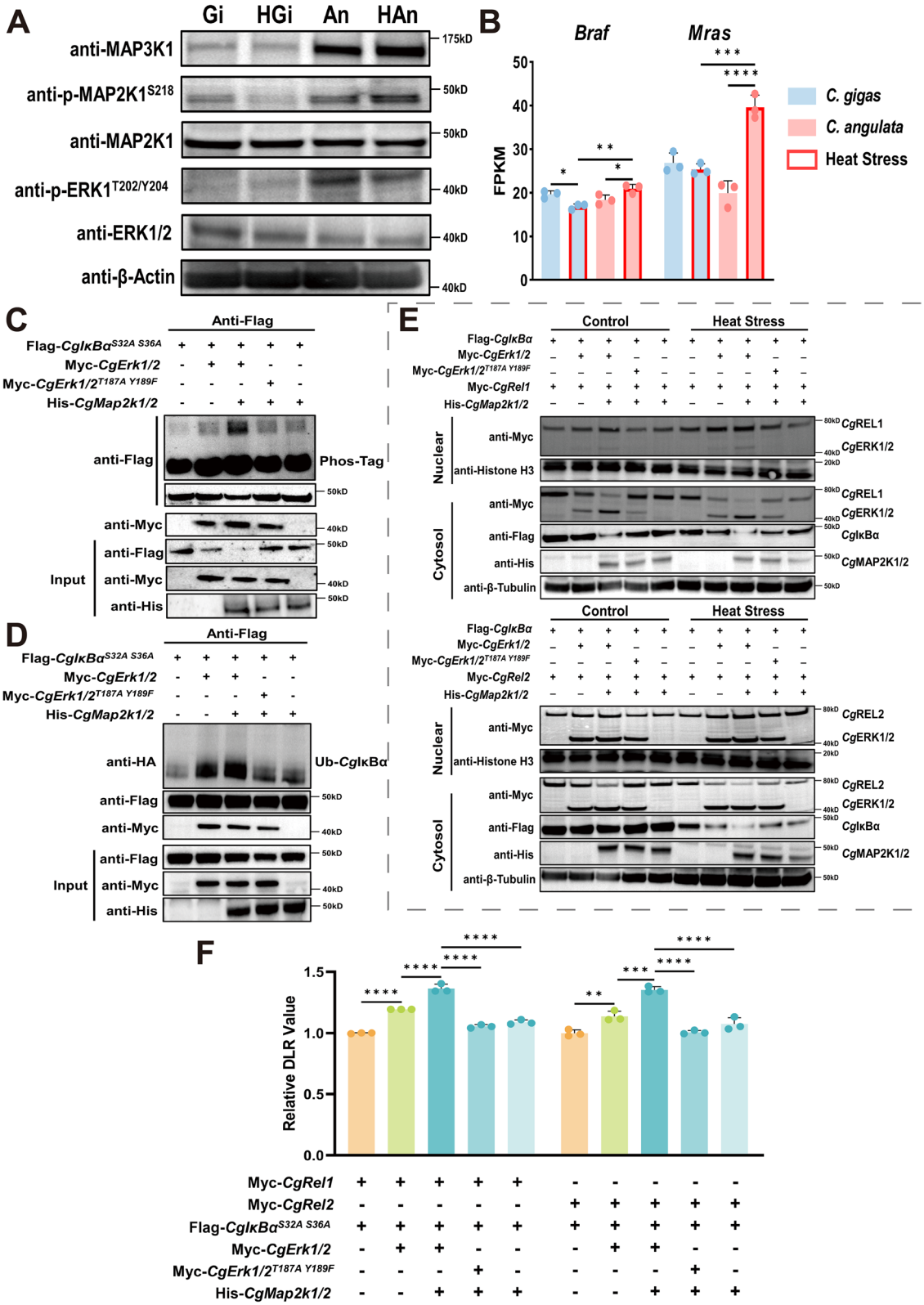

Fig. 8 (See legend on previous page.)

Using the divergent phosphorylation levels of *Cg*IκBα S74 under heat stress between *C. gigas* and *C. angulata*, in conjunction with DAP-Seq, transcriptome following RNAi experiment, and transcriptomic and ATAC-Seq data in *C. gigas* and *C. angulata* during heat stress obtained from previous study, along with experimental validations of regulatory relationship and binding affinity, we successfully identified six differentially *Cg*REL-activated genes between two species during high temperature. *Abl*, a pivotal tyrosine protein kinase, is crucial in cell survival processes such as cytoskeleton remodeling, DNA damage response, and cell apoptosis [94, 95]. *Map2k6* activates the p38MAPK signaling cascade, regulating enzyme activity (MK2 and MSK1) and transcription factor expression (p53 and ATF2), which mediate cellular survival responses under stress conditions [96–98]. Fatty acids, as essential sources and structural materials, have been extensively studied in the high-temperature stress condition [99]. *Acadm*, encoding an acyl-CoA dehydrogenase, participates in the initial step of mitochondrial fatty acid beta-oxidation, providing energy for thermal injury repair [100]. Moreover, *Cg*REL regulates *Elovl6*, a key enzyme in fatty acid metabolism that catalyzes the initial rate-limiting reaction in the elongation cycle of long-chain fatty acids, consequently impacting the synthesis of saturated fatty acids, such as C16:0 [101]. An increased ratio of saturated/unsaturated fatty acid is reportedly involved in the resistance to heat stress by regulating cell membrane fluidity, otherwise termed homeoviscous adaptation [102]. Our previous studies have also found that *C. angulata* demonstrates a higher degree of fatty acid saturation [44, 45] and a correspondingly higher heat-responsive capacity of saturated fatty acid synthesis genes [68]. Ribosomal proteins have emerged as significant markers for physiological status evaluation under stress conditions in marine organisms [103, 104]. *Eif1b* participates in the assembly of the 43S complex during the mRNA translation of protein synthesis [105], remodeling the protein landscape to enhance stress survival during heat stress [106], which is consistent with our previous findings [14]. Furthermore, *Gst*, a well-known antioxidant gene, shows increased expression and enzyme activity in marine organisms under high-temperature stress, aiding in combating oxidative stress induced by elevated temperatures [107–109]. *C. angulata* has been proven to possess a stronger anti-oxidative capacity than *C. gigas* under heat stress [14]. The differential expression patterns of the above genes in *C. gigas* and *C. angulata* under heat stress and in the North and South environments further support the activation of the MAPK/ERK-NF-κB/IκBα cascade in response to high temperature, and *C. angulata* possesses stronger activation of this cascade, which activates the expression of cellular survival, fatty acid metabolism, protein translation, and antioxidant-related genes, participating oysters' temperature adaptation.

Conclusion

The results of this study demonstrated the existence of a unique high temperature-induced crosstalk mechanism between the MAPK and NF-κB pathways in oysters. A schematic of the signal cascade of high temperature-RTK-MRAS-BRAF-MAPK-NF-κB pathways in oysters during heat stress is provided in Fig. 9E. This mechanism involved direct phosphorylation of novel Ser74 site at major *Cg*IκBα by MAPK/*Cg*ERK1/2, bypassing the Ser32 and Ser36 sites phosphorylated by IKK proteins, independently causing its ubiquitin–proteasome degradation and decreased thermal stability. The NF-κB pathway was regulated by the classical MAPK pathway, which exhibited stronger activated patterns in response to higher environmental temperature in *C. angulata* than in *C. gigas*, two allopatric congeneric oyster species with differential habitat temperatures. Finally, this signaling cascade activated cell survival, fatty acid metabolism, protein translation, and antioxidant gene

(See figure on next page.)

Fig. 9 The MAPK/ERK/IκBα/REL axis demonstrates environmental responsiveness. **A** Average Sea surface temperature of northern (Qingdao, 35°44′ N) and southern (Xiamen, 24°33′ N) sampling sites from November 2021 to January 2022. **B** The western blotting of proteins extracted from gill tissues of C. gigas and C. angulata reared at northern (Qingdao, 35°44′ N) and southern (Xiamen, 24°33′ N) sampling sites. NGi and NAn represent the C. gigas and C. angulata were reared at northern site. SGi and SAn represent the C. gigas and C. angulata were reared at southern site. **C** The relative expression of CgBraf and CgMras of C. gigas and C. angulata reared at northern (Qingdao, 35°44′ N) and southern (Xiamen, 24°33′ N) sampling sites. **D** The relative expression of CgREL-mediated downstream genes (CgBraf and CgMras) of C. gigas and C. angulata reared at northern (Qingdao, 35°44′ N) and southern (Xiamen, 24°33′ N) sampling sites. **E** Schematic representation of novel ERK/IκBα/REL axis of oyster in facing high temperature. Under thermal stress, the MAPK pathway is activated via RTKs-CgMRAS complex. Then, the CgMAP2K1/2 is phosphorylated by CgBRAF or CgMAP3K1 at Ser238 and Ser242 sites, which exerts kinase activity to phosphorylate CgERK1/2 at Thr187 and Tyr189 sits. Subsequently, CgERK1/2 phosphorylates CgIκBα at the S74 site, facilitating its ubiquitin–proteasome degradation and releasing CgREL1 and CgREL2 for nuclear translocation, which as a transcription factor, activating genes involved in cell survival, fatty acid metabolism, protein translation, and antioxidant responses to assist oysters in combating heat stress

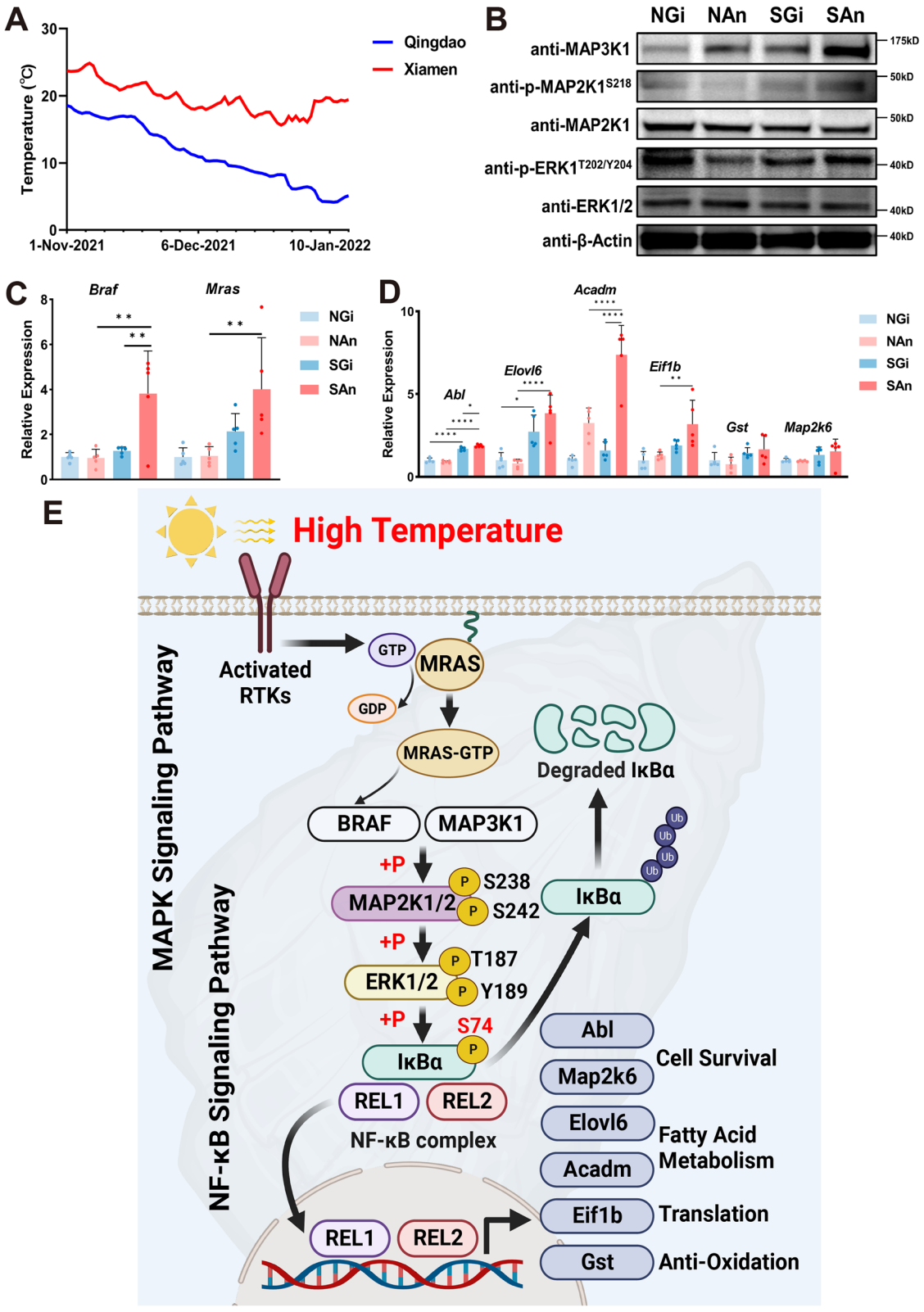

Fig. 9 (See legend on previous page.)

expression by promoting *Cg*REL nuclear translocation to resist heat stress. These findings highlight the presence of complex and unique phosphorylation-mediated regulatory networks in marine invertebrates, which differ from the established mechanisms in vertebrates and contribute to expanding our understanding of the evolution and function of the crosstalk mechanisms between existing classical pathways.

Supplementary Information

The online version contains supplementary material available at https://doi.org/10.1186/s12964-024-01923-0.

Supplementary Material 1.

Supplementary Material 2.

Supplementary Material 3.

Supplementary Material 4.

Supplementary Material 5.

Acknowledgements
The authors would like to thank the supercomputer cluster of the High-Performance Computing Center (HPCC) at the Institute of Oceanology, Chinese Academy of Sciences for support in bioinformatics analysis. This research was funded by the National Key R&D Program of China (No. 2022YFD2400304), Key Research and Development Program of Shandong (2022LZGC015; ZFJH202309), and China Agriculture Research System of MOF and MARA (No. CARS-49).

Authors' contributions
Conceptualization, L.L. and G.Z.; Validation, C.W., Z. J., M.D., T.Z. and J.C; Formal Analysis, C.W.; Investigation, C.W.; Writing – Original Draft, C.W. and Z. J.; Writing – Review & Editing, L.L. and G.Z.; Funding Acquisition, L.L. and G.Z.; Visualization, C.W.; Supervision, L.L. and G.Z.

Funding
This research was funded by the National Key R&D Program of China (No. 2022YFD2400304), Key Research and Development Program of Shandong (2022LZGC015; ZFJH202309), and China Agriculture Research System of MOF and MARA (No. CARS-49).

Data availability
The raw sequencing data of transcriptome in RNAi experiment and DAP-Seq in this study have been deposited the Sequence Read Archive (SRA) BioProject under the accession number: PRJNA1059049 and PRJNA1058704.

Declarations

Competing interests
The authors declare no competing interests.

Received: 30 June 2024 Accepted: 1 November 2024
Published online: 11 November 2024

References

1. Yoshihara T, Naito H, Kakigi R, Ichinoseki-Sekine N, Ogura Y, Sugiura T, Katamoto S. Heat stress activates the Akt/mTOR signalling pathway in rat skeletal muscle. Acta Physiol. 2013;207:416–26.
2. Kamal MM, Ishikawa S, Takahashi F, Suzuki K, Kamo M, Umezawa T, Shinozaki K, Kawamura Y, Uemura M. Large-scale phosphoproteomic study of arabidopsis membrane proteins reveals early signaling events in response to cold. Int J Mol Sci. 2020;21(22):8631.
3. Huang J, Wu Z, Zhang X. Short-term mild temperature-stress-induced alterations in the C. elegans phosphoproteome. Int J Mol Sci. 2020;21(17):6409.
4. Kanshin E, Kubiniok P, Thattikota Y, D'Amours D, Thibault P. Phosphoproteome dynamics of Saccharomyces cerevisiae under heat shock and cold stress. Mol Syst Biol. 2015;11:813–813.
5. Zhao Y, Hu X, Liu Y, Dong S, Wen Z, He W, Zhang S, Huang Q, Shi M. ROS signaling under metabolic stress: cross-talk between AMPK and AKT pathway. Mol Cancer. 2017;16:79.
6. Gonzalez A, Hall MN, Lin SC, Hardie DG. AMPK and TOR: The Yin and Yang of cellular nutrient sensing and growth control. Cell Metab. 2020;31:472–92.
7. Oehler-Jänne C. Bueren AOv, Vuong V, Hollenstein A, Grotzer MA, Pruschy M: Temperature sensitivity of phospho-Ser473-PKB/AKT. Biochem Biophys Res Commun. 2008;375:399–404.
8. Paszek A, Kardyńska M, Bagnall J, Śmieja J, Spiller DG, Widłak P, Kimmel M, Widlak W, Paszek P. Heat shock response regulates stimulus-specificity and sensitivity of the pro-inflammatory NF-κB signalling. Cell Communication and Signaling. 2020;18:77.
9. Harper CV, Woodcock DJ, Lam C, Garcia-Albornoz M, Adamson A, Ashall L, Rowe W, Downton P, Schmidt L, West S, et al. Temperature regulates NF-κB dynamics and function through timing of A20 transcription. Proc Natl Acad Sci. 2018;115:E5243–9.
10. Moustafa K, AbuQamar S, Jarrar M, Al-Rajab AJ, Trémouillaux-Guiller J. MAPK cascades and major abiotic stresses. Plant Cell Rep. 2014;33:1217–25.
11. Evans TG, Somero GN. Phosphorylation events catalyzed by major cell signaling proteins differ in response to thermal and osmotic stress among native (Mytilus californianus and Mytilus trossulus) and invasive (Mytilus galloprovincialis) species of mussels. Physiol Biochem Zool. 2010;83:984–96.
12. Michaelidis B, Hatzikamari M, Antoniou V, Anestis A, Lazou A. Stress activated protein kinases, JNKs and p38 MAPK, are differentially activated in ganglia and heart of land snail Helix lucorum (L.) during seasonal hibernation and arousal. Comp Biochem Physiol Part A: Mol Integr Physiol. 2009;153(2):149–53.
13. Yao C-L, Somero GN. Thermal stress and cellular signaling processes in hemocytes of native (Mytilus californianus) and invasive (M. galloprovincialis) mussels: Cell cycle regulation and DNA repair. Comp Biochem Physiol Part A: Mol Integr Physiol. 2013;165:159–68.
14. Wang C, Du M, Jiang Z, Cong R, Wang W, Zhang G, Li L. Comparative proteomic and phosphoproteomic analysis reveals differential heat response mechanism in two congeneric oyster species. Ecotoxicol Environ Saf. 2023;263:115197.
15. Sun S-C, Ley SC. New insights into NF-κB regulation and function. Trends Immunol. 2008;29:469–78.
16. Ghosh S, Hayden MS. New regulators of NF-κB in inflammation. Nat Rev Immunol. 2008;8:837–48.
17. Hayden MS, Ghosh S. Shared principles in NF-κB signaling. Cell. 2008;132:344–62.
18. Zheng C, Yin Q, Wu H. Structural studies of NF-κB signaling. Cell Res. 2011;21:183–95.
19. Siebenlist U, Franzoso G, Brown K. Structure, regulation and function of NF-kappaB. Annu Rev Cell Biol. 1994;10:405–55.
20. Hayden MS, Ghosh S. NF-κB, the first quarter-century: remarkable progress and outstanding questions. Genes Dev. 2012;26:203–34.
21. Hinz M, Arslan SÇ, Scheidereit C. It takes two to tango: IκBs, the multifunctional partners of NF-κB. Immunol Rev. 2012;246:59–76.
22. Chen J, Chen ZJ. Regulation of NF-κB by ubiquitination. Curr Opin Immunol. 2013;25:4–12.
23. Perkins ND. Post-translational modifications regulating the activity and function of the nuclear factor kappa B pathway. Oncogene. 2006;25:6717–30.
24. Li C, Wang S, He J. The two NF-κB pathways regulating bacterial and WSSV infection of shrimp. Front Immunol. 2019;10:1785.
25. Xu F, Li J, Zhang Y, Li X, Zhang Y, Xiang Z, Yu Z. CgIκB3, the third novel inhibitor of NF-kappa B (IκB) protein, is involved in the immune defense of the Pacific oyster. Crassostrea gigas Fish & Shellfish Immunology. 2015;46:648–55.

26. Sang X, Dong J, Chen F, Wei L, Liu Y, Zhang M, Huang B, Wang X. Molecular cloning and immune function study of an oyster IκB gene in the NF-κB signaling pathway. Aquaculture. 2020;525:735322.
27. Dong J, Sang X, Song H, Zhan R, Wei L, Liu Y, Zhang M, Huang B, Wang X. Molecular characterization and functional analysis of a Rel gene in the Pacific oyster. Fish Shellfish Immunol. 2020;101:9–18.
28. Oyanedel D, Gonzalez R, Flores-Herrera P, Brokordt K, Rosa RD, Mercado L, Schmitt P. Molecular characterization of an inhibitor of NF-κB in the scallop Argopecten purpuratus: First insights into its role on antimicrobial peptide regulation in a mollusk. Fish Shellfish Immunol. 2016;52:85–93.
29. Zhang D, Jiang S, Qiu L, Su T, Wu K, Li Y, Zhu C, Xu X. Molecular characterization and expression analysis of the IκB gene from pearl oyster Pinctada fucata. Fish Shellfish Immunol. 2009;26:84–90.
30. Goodson Michael S, Kojadinovic M, Troll Joshua V, Scheetz Todd E, Casavant Thomas L, Soares MB, McFall-Ngai Margaret J. Identifying components of the NF-κB pathway in the beneficial Euprymna scolopes-Vibrio fischeri light organ symbiosis. Appl Environ Microbiol. 2005;71:6934–46.
31. Khush RS, Leulier F, Lemaitre B. Drosophila immunity: two paths to NF-κB. Trends Immunol. 2001;22:260–4.
32. Kasthuri SR, Whang I, Navaneethaiyer U, Lim B-S, Choi CY, Lee J. Molecular characterization and expression analysis of IκB from Haliotis discus discus. Fish Shellfish Immunol. 2013;34:1596–604.
33. Li Q, Verma IM. NF-κB regulation in the immune system. Nat Rev Immunol. 2002;2:725–34.
34. Liu T, Zhang L, Joo D, Sun S-C. NF-κB signaling in inflammation. Signal Transduct Target Ther. 2017;2:17023.
35. Karin M. Nuclear factor-κB in cancer development and progression. Nature. 2006;441:431–6.
36. Moniruzzaman M, Ghosal I, Das D, Chakraborty SB. Melatonin ameliorates H2O2-induced oxidative stress through modulation of Erk/Akt/NFkB pathway. Biol Res. 2018;51:17.
37. Montagnani C, Labreuche Y, Escoubas JM. Cg-IκB, a new member of the IκB protein family characterized in the pacific oyster Crassostrea gigas. Dev Comp Immunol. 2008;32:182–90.
38. Zhang G, Fang X, Guo X, Li L, Luo R, Xu F, Yang P, Zhang L, Wang X, Qi H, et al. The oyster genome reveals stress adaptation and complexity of shell formation. Nature. 2012;490:49–54.
39. Guo X. Use and exchange of genetic resources in molluscan aquaculture. Rev Aquac. 2009;1:251–9.
40. Clark MS, Thorne MAS, Amaral A, Vieira F, Batista FM, Reis J, Power DM. Identification of molecular and physiological responses to chronic environmental challenge in an invasive species: the Pacific oyster. Crassostrea gigas Ecology and Evolution. 2013;3:3283–97.
41. Haiyan W, Guofan Z, Xiao L, Ximing G. Classification of common oysters from North China. J Shellfish Res. 2008;27:495–503.
42. Ren J, Liu X, Jiang F, Guo X, Liu B. Unusual conservation of mitochondrial gene order in Crassostreaoysters: evidence for recent speciation in Asia. BMC Evol Biol. 2010;10:394.
43. Ghaffari H, Wang W, Li A, Zhang G, Li L. Thermotolerance Divergence Revealed by the Physiological and Molecular Responses in Two Oyster Subspecies of Crassostrea gigas in China. Front Physiol. 2019;10:1137.
44. Wang C, Li A, Wang W, Cong R, Wang L, Zhang G, Li L. Integrated application of transcriptomics and metabolomics reveals the energy allocation-mediated mechanisms of growth-defense trade-offs in Crassostrea gigas and Crassostrea angulata. Front Marine Sci. 2021;8:744626.
45. Wang C, Li A, Cong R, Qi H, Wang W, Zhang G, Li L. Cis- and trans-variations of stearoyl-CoA desaturase provide new insights into the mechanisms of diverged pattern of phenotypic plasticity for temperature adaptation in two congeneric oyster species. Mol Biol Evol. 2023;40:msad015.
46. Sanford E, Kelly MW. Local adaptation in marine invertebrates. Ann Rev Mar Sci. 2011;3:509–35.
47. Chen C, Chen H, Zhang Y, Thomas HR, Frank MH, He Y, Xia R. TBtools: an integrative toolkit developed for interactive analyses of big biological data. Mol Plant. 2020;13:1194–202.
48. Zhang D, Gao F, Jakovlić I, Zou H, Zhang J, Li WX, Wang GT. PhyloSuite: An integrated and scalable desktop platform for streamlined molecular sequence data management and evolutionary phylogenetics studies. Mol Ecol Resour. 2020;20:348–55.
49. Kalyaanamoorthy S, Minh BQ, Wong TKF, von Haeseler A, Jermiin LS. ModelFinder: fast model selection for accurate phylogenetic estimates. Nat Methods. 2017;14:587–9.
50. Minh BQ, Schmidt HA, Chernomor O, Schrempf D, Woodhams MD, von Haeseler A, Lanfear R. IQ-TREE 2: new models and efficient methods for phylogenetic inference in the genomic era. Mol Biol Evol. 2020;37:1530–4.
51. Zhang L, Li L, Guo X, Litman GW, Dishaw LJ, Zhang G. Massive expansion and functional divergence of innate immune genes in a protostome. Sci Rep. 2015;5:8693.
52. Qi H, Li L, Zhang G. Construction of a chromosome-level genome and variation map for the Pacific oyster Crassostrea gigas. Mol Ecol Resour. 2021;21:1670–85.
53. Patro R, Duggal G, Love MI, Irizarry RA, Kingsford C. Salmon provides fast and bias-aware quantification of transcript expression. Nat Methods. 2017;14:417–9.
54. Yang Z. PAML 4: Phylogenetic analysis by maximum likelihood. Mol Biol Evol. 2007;24:1586–91.
55. Xu B, Yang Z. pamlX: A graphical user interface for PAML. Mol Biol Evol. 2013;30:2723–4.
56. Bolger AM, Lohse M, Usadel B. Trimmomatic: a flexible trimmer for Illumina sequence data. Bioinformatics. 2014;30:2114–20.
57. Kim D, Langmead B, Salzberg SL. HISAT: a fast spliced aligner with low memory requirements. Nat Methods. 2015;12:357–60.
58. Anders S, Pyl PT, Huber W. HTSeq—a Python framework to work with high-throughput sequencing data. Bioinformatics. 2015;31:166–9.
59. Love MI, Huber W, Anders S. Moderated estimation of fold change and dispersion for RNA-seq data with DESeq2. Genome Biol. 2014;15:550.
60. Bartlett A, O'Malley RC. Huang S-sC, Galli M, Nery JR, Gallavotti A, Ecker JR: Mapping genome-wide transcription-factor binding sites using DAP-seq. Nat Protoc. 2017;12:1659–72.
61. Langmead B, Salzberg SL. Fast gapped-read alignment with Bowtie 2. Nat Methods. 2012;9:357–9.
62. Ramírez F, Ryan DP, Grüning B, Bhardwaj V, Kilpert F, Richter AS, Heyne S, Dündar F, Manke T. deepTools2: a next generation web server for deep-sequencing data analysis. Nucleic Acids Res. 2016;44:W160–5.
63. Zhang Y, Liu T, Meyer CA, Eeckhoute J, Johnson DS, Bernstein BE, Nusbaum C, Myers RM, Brown M, Li W, Liu XS. Model-based Analysis of ChIP-Seq (MACS). Genome Biol. 2008;9:R137.
64. Yu G, Wang L-G, He Q-Y. ChIPseeker: an R/Bioconductor package for ChIP peak annotation, comparison and visualization. Bioinformatics. 2015;31:2382–3.
65. Thorvaldsdóttir H, Robinson JT, Mesirov JP. Integrative Genomics Viewer (IGV): high-performance genomics data visualization and exploration. Brief Bioinform. 2013;14:178–92.
66. Livak KJ, Schmittgen TD. Analysis of relative gene expression data using real-time quantitative PCR and the 2(-Delta Delta C(T)) Method. Methods. 2001;25:402–8.
67. Song C, Ye M, Liu Z, Cheng H, Jiang X, Han G, Songyang Z, Tan Y, Wang H, Ren J, et al. Systematic analysis of protein phosphorylation networks from phosphoproteomic data. Molecular & cellular proteomics : MCP. 2012;11:1070–83.
68. Wang C, Jiang Z, Du M, Li Q, Cong R, Wang W, Zhang G, Li L. Comparative chromatin dynamics reveal differential thermal tolerance mechanisms between two congeneric oyster species. Aquaculture. 2024;579:740177.
69. Katayama H, Sasai K, Kawai H, Yuan Z-M, Bondaruk J, Suzuki F, Fujii S, Arlinghaus RB, Czerniak BA, Sen S. Phosphorylation by aurora kinase A induces Mdm2-mediated destabilization and inhibition of p53. Nat Genet. 2004;36:55–62.
70. Lavoie H, Gagnon J, Therrien M. ERK signalling: a master regulator of cell behaviour, life and fate. Nat Rev Mol Cell Biol. 2020;21:607–32.
71. Lin G, Tang Z, Ye Y-B, Chen Q. NF-κB activity is downregulated by KRAS knockdown in SW620 cells via the RAS-ERK-IκBα pathway. Oncol Rep. 2012;27:1527–34.
72. Funakoshi M, Tago K, Sonoda Y, Tominaga S-i, Kasahara T. A MEK Inhibitor, PD98059 Enhances IL-1-Induced NF-κB activation by the enhanced and sustained degradation of IκBα. Biochem Biophys Res Commun. 2001;283:248–54.
73. Liu YQ, You S. Tashiro S-i, Onodera S, Ikejima T: Roles of Ras and extracellular signal-regulated kinase-dependent IκBα degradation

in oridonin-enhanced phagocytosis of apoptotic cells by human macrophage-like U937 cells. Int Immunopharmacol. 2006;6:260–8.
74. Chen B-C, Yu C-C, Lei H-C, Chang M-S, Hsu M-J, Huang C-L, Chen M-C, Sheu J-R, Chen T-F, Chen T-L, et al. Bradykinin B2 receptor mediates NF-κB activation and cyclooxygenase-2 expression via the Ras/Raf-1/ERK pathway in human airway epithelial cells1. J Immunol. 2004;173:5219–28.
75. Green Charlotte J, Macrae K, Fogarty S, Hardie DG, Sakamoto K, Hundal Harinder S. Counter-modulation of fatty acid-induced pro-inflammatory nuclear factor κB signalling in rat skeletal muscle cells by AMP-activated protein kinase. Biochemical Journal. 2011;435:463–74.
76. Maeng Y-S, Min J-K, Kim JH, Yamagishi A, Mochizuki N, Kwon J-Y, Park Y-W, Kim Y-M, Kwon Y-G. ERK is an anti-inflammatory signal that suppresses expression of NF-κB-dependent inflammatory genes by inhibiting IKK activity in endothelial cells. Cell Signal. 2006;18:994–1005.
77. Yeh PY, Yeh K-H, Chuang S-E, Song YC, Cheng A-L. Suppression of MEK/ERK signaling pathway enhances cisplatin-induced NF-κB activation by protein phosphatase 4-mediated NF-κB p65 Thr dephosphorylation. J Biol Chem. 2004;279:26143–8.
78. He G, Xiong X, Peng Y, Yang C, Xu Y, Liu X, Liang J, Masanja F, Yang K, Xu X, et al. Transcriptomic responses reveal impaired physiological performance of the pearl oyster following repeated exposure to marine heatwaves. Sci Total Environ. 2023;854: 158726.
79. Liu Y, Li L, Yang J, Huang H, Song W. Transcriptome analysis reveals genes connected to temperature adaptation in juvenile antarctic krill Euphausia superba. Genes & Genomics. 2023;45:1063–71.
80. Anestis A, Lazou A, Pörtner HO, Michaelidis B. Behavioral, metabolic, and molecular stress responses of marine bivalve Mytilus galloprovincialis during long-term acclimation at increasing ambient temperature. American Journal of Physiology-Regulatory, Integrative and Comparative Physiology. 2007;293:R911–21.
81. Xu L, Wang Y, Lin S, Li H, Qi P, Buttino I, Wang W, Guo B. Insights into the response in digestive gland of Mytilus coruscus under heat stress using TMT-based proteomics. In Animals. 2023;13(14):2248.
82. Keller JM, Escara-Wilke JF, Keller ET. Heat stress-induced heat shock protein 70 expression is dependent on ERK activation in zebrafish (Danio rerio) cells. Comp Biochem Physiol A: Mol Integr Physiol. 2008;150:307–14.
83. Yang S, Zhao T, Ma A, Huang Z, Yang J, Yuan C, Guo X, Zhu C. Heat stress-induced HSP90 expression is dependent on ERK and HSF1 activation in turbot (Scophthalmus maximus) kidney cells. Cell Stress Chaperones. 2021;26:173–85.
84. Wang Y, Wu J, Xia S-W, Zhao F, Ding Q, Ye X-M, Zhong J-F, Chen K-L, Wang H-L. miR-27a-3p relieves heat stress-induced mitochondrial damage and aberrant milk protein synthesis through MEK/ERK pathway in BMECs. Cell Stress Chaperones. 2023;28:265–74.
85. Wu J, Ibtisham F, Niu YF, Wang Z, Li GH, Zhao Y, Nawab A, Xiao M, An L. Curcumin inhibits heat-induced oxidative stress by activating the MAPK-Nrf2 / ARE signaling pathway in chicken fibroblasts cells. J Therm Biol. 2019;79:112–9.
86. Siddiqui SH, Khan M, Park J, Lee J, Choe H, Shim K, Kang D. COPA3 peptide supplementation alleviates the heat stress of chicken fibroblasts. Front Vet Sci. 2023;10:985040.
87. Kinoshita T, Yoshida I, Nakae S, Okita K, Gouda M, Matsubara M, Yokota K, Ishiguro H, Tada T. Crystal structure of human mono-phosphorylated ERK1 at Tyr204. Biochem Biophys Res Commun. 2008;377:1123–7.
88. Lavoie H, Sahmi M, Maisonneuve P, Marullo SA, Thevakumaran N, Jin T, Kurinov I, Sicheri F, Therrien M. MEK drives BRAF activation through allosteric control of KSR proteins. Nature. 2018;554:549–53.
89. Yao B, Zhang Y, Delikat S, Mathias S, Basu S, Kolesnick R. Phosphorylation of Raf by ceramide-activated protein kinase. Nature. 1995;378:307–10.
90. Kwon JJ, Hajian B, Bian Y, Young LC, Amor AJ, Fuller JR, Fraley CV, Sykes AM, So J, Pan J, et al. Structure–function analysis of the SHOC2–MRAS–PP1C holophosphatase complex. Nature. 2022;609:408–15.
91. Lin RZ, Hu Z-W, Chin JH, Hoffman BB. Heat shock activates c-Src tyrosine kinases and phosphatidylinositol 3-Kinase in NIH3T3 fibroblasts. J Biol Chem. 1997;272:31196–202.
92. Zhang Y, He X, Yu Z. Two homologues of inhibitor of NF-kappa B (IκB) are involved in the immune defense of the Pacific oyster. Crassostrea gigas Fish & Shellfish Immunology. 2011;30:1354–61.
93. Liu Y-L, Ding K-N, Shen X-L, Liu H-X, Zhang Y-A, Liu Y-Q, He Y-M, Tang L-P. Chronic heat stress promotes liver inflammation in broilers via enhancing NF-κB and NLRP3 signaling pathway. BMC Vet Res. 2022;18:289.
94. Gu JJ, Lavau CP, Pugacheva E, Soderblom EJ, Moseley MA, Pendergast AM. Abl family kinases modulate T cell-mediated inflammation and chemokine-induced migration through the adaptor HEF1 and the GTPase Rap1. Sci Signal. 2012;5(233):ra51.
95. Wie SM, Adwan TS, DeGregori J, Anderson SM, Reyland ME. Inhibiting tyrosine phosphorylation of protein kinase Cδ (PKCδ) protects the salivary gland from radiation damage. J Biol Chem. 2014;289:10900–8.
96. Shi G-X, Jin L, Andres DA. A Rit GTPase-p38 mitogen-activated protein kinase survival pathway confers resistance to cellular stress. Mol Cell Biol. 2011;31:1938–48.
97. Chan SHH, Hsu K-S, Huang C-C, Wang L-L, Ou C-C, Chan JYH. NADPH oxidase-derived superoxide anion mediates angiotensin II–induced pressor effect via activation of p38 mitogen-activated protein kinase in the rostral ventrolateral medulla. Circ Res. 2005;97:772–80.
98. Gutiérrez-Uzquiza Á, Arechederra M, Bragado P, Aguirre-Ghiso JA, Porras A. p38α mediates cell survival in response to oxidative stress via induction of antioxidant genes: effect on the p70S6K pathway. J Biol Chem. 2012;287:2632–42.
99. Iba K. Acclimative response to temperature stress in higher plants: approaches of gene Engineering for temperature tolerance. Annu Rev Plant Biol. 2002;53:225–45.
100. He M, Pei Z, Mohsen A-W, Watkins P, Murdoch G, Van Veldhoven PP, Ensenauer R, Vockley J. Identification and characterization of new long chain Acyl-CoA dehydrogenases. Mol Genet Metab. 2011;102:418–29.
101. Ohno Y, Suto S, Yamanaka M, Mizutani Y, Mitsutake S, Igarashi Y, Sassa T, Kihara A. ELOVL1 production of C24 acyl-CoAs is linked to C24 sphingolipid synthesis. Proc Natl Acad Sci. 2010;107:18439–44.
102. Mendoza Dd. Temperature sensing by membranes. Annu Rev Microbiol. 2014;68:101–16.
103. Jiao L, Dai T, Jin M, Sun P, Zhou Q. Transcriptome analysis of the hepatopancreas in the litopenaeus vannamei responding to the lead stress. Biol Trace Elem Res. 2021;199:1100–9.
104. Vieira JCS, Braga CP, de Oliveira G, Padilha CdCF, de Moraes PM, Zara LF, Leite AdL, Buzalaf MAR, Padilha PdM. Mercury exposure: protein biomarkers of mercury exposure in Jaraqui fish from the Amazon region. Biol Trace Elem Res. 2018;183:164–71.
105. Sun Y-L, Gong H-S, Jin C-W, Hong S-K. Molecular cloning and identification of eukaryotic translation initiation factor 1 family genes (eIF1, eIF1A and eIF1B) in Leymus chinensis (Trin.). Biotechnol Biotechnol Equip. 2015;29:609–16.
106. Neef DW, Thiele DJ. Enhancer of decapping proteins 1 and 2 are important for translation during heat stress in Saccharomyces cerevisiae. Mol Microbiol. 2009;73:1032–42.
107. Guerriero G, Bassem SM, Khalil WKB, Temraz TA, Ciarcia G, Gawad FKA. Temperature changes and marine fish species (Epinephelus coioides and Sparus aurata): Role of oxidative stress biomarkers in toxicological food studies. Emirates Journal of Food and Agriculture. 2018;30:205–11.
108. Teixeira T, Diniz M, Calado R, Rosa R. Coral physiological adaptations to air exposure: Heat shock and oxidative stress responses in Veretillum cynomorium. J Exp Mar Biol Ecol. 2013;439:35–41.
109. Missionário M, Travesso M, Calado R, Madeira D. Cellular stress response and acclimation capacity of the ditch shrimp Palaemon varians to extreme weather events - How plastic can a plastic species be? Sci Total Environ. 2023;856: 158732.

Publisher's Note